

Thesis - UH

The structure of the east rift zone of K
AC .H3 no.B77 15257



Broyles, Michael
SOEST Library

THESIS

070
B70
Str
ms

THE STRUCTURE OF THE EAST RIFT ZONE
OF KILAUEA, HAWAII FROM
SEISMIC REFRACTION, GRAVITY AND MAGNETIC SURVEYS

A THESIS SUBMITTED TO THE GRADUATE DIVISION OF THE
UNIVERSITY OF HAWAII IN PARTIAL FULFILLMENT
OF THE REQUIREMENTS FOR THE DEGREE OF

MASTER OF SCIENCE

IN GEOLOGY AND GEOPHYSICS

DECEMBER 1977

by

Michael L. Broyles

Thesis Committee:

Augustine S. Furumoto, Chairman
Gordon A. Macdonald
Michael O. Garcia

We certify that we have read this thesis and that in our opinion it is satisfactory in scope and quality as a thesis for the degree of Master of Science in Geology and Geophysics.

THESIS COMMITTEE

Augustine S. Furumoto
Chairman

Jordan P. MacDonald

Michael O. Garcia

ACKNOWLEDGMENTS

The author wishes to thank Dr. A. S. Furumoto for his helpful guidance as well as allowing me to assume a major role in organizing the 1977 Puna refraction survey from which this thesis draws a large amount of data.

The 1977 Puna refraction survey could not have been successfully completed without the help of the following people: Dr. Charles Helsley for his role in directing the field operations and helpful advice in reducing the data, Carroll Dodd for assembling and operating the array network and communications center, Edward Sakoda, Roger Norris and Patrick Lineberger for assisting with the field work and Pete Pozzi and Lee Smith for operating the scientific equipment on board the boat.

A special thanks to Candy Fenander, Douglas Klein and Wayne Suyenaga for their helpful comments in drafting this thesis and my committee members Dr. Gordon A. Macdonald and Dr. Michael O. Garcia for their guidance.

ABSTRACT

This study of the crustal structure beneath the east rift zone of Kilauea utilizes new refraction data as well as existing gravity and magnetic data as geophysical constraints.

The purpose of this thesis is to interpret the structure within the east rift outlining the arrangement of the dike intrusions and their relationship to the regional crustal structure.

Previous studies of the crustal structure of Hawaii have either used long refraction lines that could not delineate the fine structure in the rift zones or short refraction lines unable to penetrate to the depths of the higher velocity material comprising the intrusive dike complex. By using seismic refraction data from the 1977 survey along with gravity and magnetic data from previous surveys, the nature of the intrusive complex in the Puna region of Hawaii has been resolved.

From this study, it is concluded that the depth to the top of the intrusive complex averages 2-3 km, reaching only 1 km in certain regions. It is also concluded that the lower depths of the intrusion average 4-5 km. This analysis suggests that the subsurface lateral extent of the rift complex is much wider, 12-17 km, than the surface expression would indicate.

A northward dip of 6-7 degrees on the upper surface of the main dike structure is compatible with the seismic refraction and gravity data and suggests either, lateral development of the rift to the

south as successively younger dikes intrude at shallower depths and
or the development of the younger east rift complex to the south on
top of the older Mauna Loa rift zone on the north.

TABLE OF CONTENTS

	Page
ACKNOWLEDGMENTS	iii
ABSTRACT	iv
LIST OF TABLES	vii
LIST OF FIGURES	viii
INTRODUCTION	1
PREVIOUS INVESTIGATIONS	7
FIELD DATA	10
DATA REDUCTION AND ANALYSIS	16
SEISMIC REFRACTION RESULTS	30
GRAVITY DATA AND ANALYSIS	46
DISCUSSION	60
COMPARISON WITH MAGNETIC DATA	60
COMPARISON WITH PASSIVE SEISMICS	61
COMPARISON WITH PETROLOGY	70
CONCLUSIONS REGARDING THE STRUCTURE OF THE EAST RIFT	75
REFERENCES	83

LIST OF TABLES

Table		Page
1	Travel Times for the 1977 East Rift Refraction	45

LIST OF FIGURES

Figure		Page
1	The east rift zone of Hawaii	3
2	Map of Puna with shot points and receiver locations	12
3	The NS line TEAC 1 (T1) seismograms showing P, T and sonobuoy arrivals	19
4	Sonobuoy and T-phase arrivals for the NS line	21
5	Sonobuoy and T-phase arrivals for the EW line	23
6	Bathymetry of the Puna submarine ridge	26
7	The travel-time plots for the EW line shots 2-5	32
8	The travel-time plots for the NS line shots 1-7	34
9	The travel time plots for the TEAC 1 and TEAC 2 locations on the EW line	36
10	Crustal sections from seismic refraction	44
11	Bouguer gravity map of Puna, Hawaii	48
12	Kinoshita's Bouguer map of the island of Hawaii	51
13	Gravity models for line B'-B	55
14	Gravity models for line A'-A	58
15	Magnetic anomalies over the Puna submarine ridge for sea and land	62
16	Magnetic anomalies over the Puna region	64
17	Depth of foci of microearthquakes	68
18	Petrology and velocity structure of the east rift	73
19	Structure of the rift complex	82

INTRODUCTION

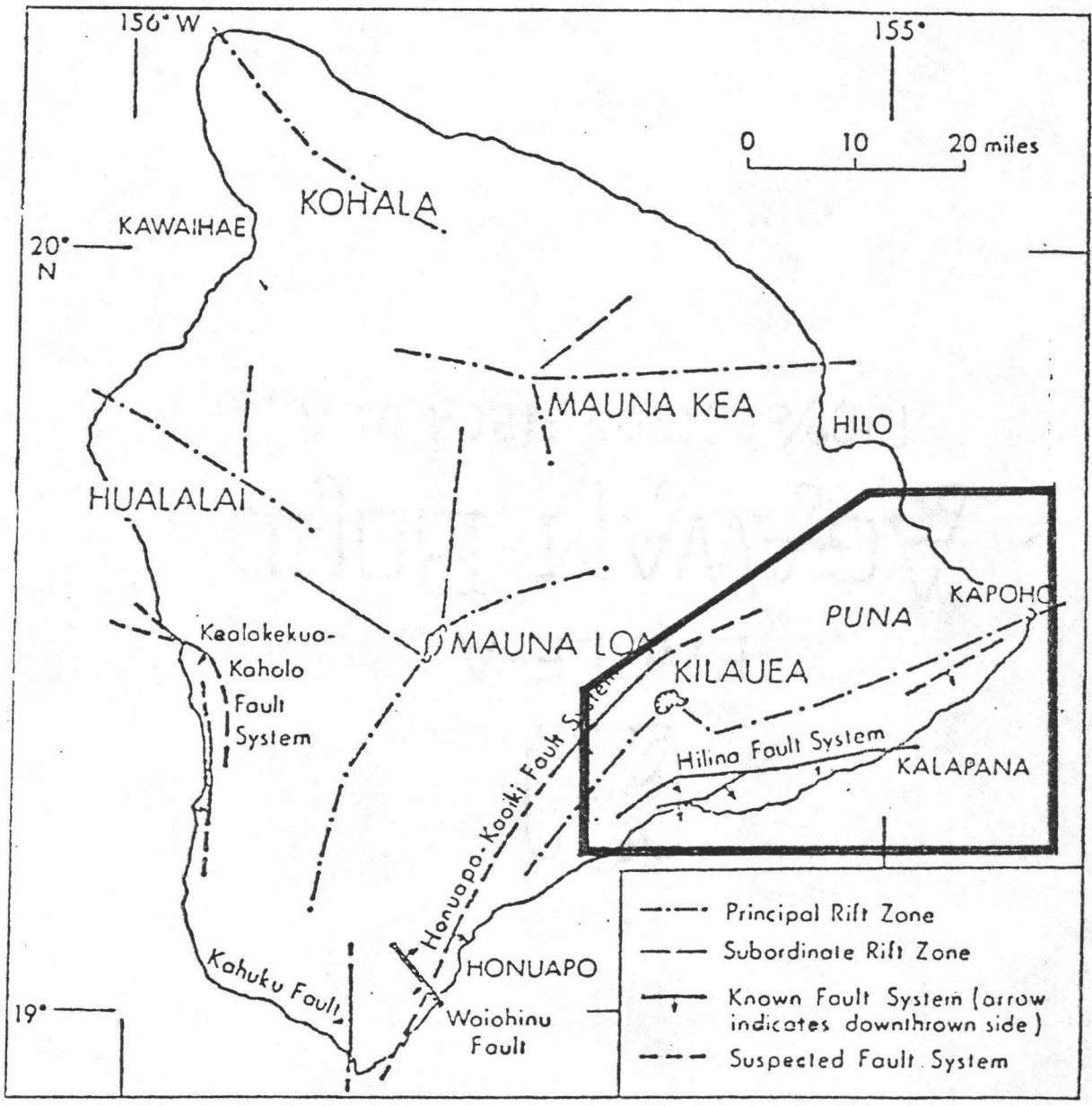
Geophysical investigations of the east rift zone of Kilauea, Hawaii have been an integral part of the Hawaii Geothermal Project since its commencement in 1973. Various geophysical surveys by the Hawaii Institute of Geophysics conducted up until January 1977 have included electromagnetics (Klein, 1976), magnetics (Norris, 1976), gravity (Furumoto, 1976) and seismic refraction (Suyenaga, 1976).

The purpose of this thesis is to update the geophysical studies now that the 1977 Puna refraction has been completed. This refraction project recorded two lines in an attempt to outline the lateral extent of the east rift as well as to determine the depth of the intrusive anomaly or main dike complex.

The landward expression of the east rift extends for more than 60 km from the summit of Kilauea volcano to Cape Kumukahi (Fig. 1). The seaward expression of the east rift extends for another 60-80 km from Cape Kumukahi northeastward to a possible merge with the Molokai Fracture Zone (Macdonald, personal communication, 1977). Studies by Malahoff and McCoy (1967) indicate that the seaward expression of the rift is characterized by high gravity and magnetic values.

Within the landward expression of the rift zone, four distinct surface features are observed and when well developed in one place as in the Kolaie fault system, they are found in this order from north to south (Moore and Krivoy, 1964): (1) the eruptive fissures,

Figure 1. The Island of Hawaii from Macdonald (1956) and the east rift.



(2) the eruptive cones, (3) the pit craters, (4) the fault scarps. These features are aligned in a northeasterly direction forming the dominant trend of the rift zone (Fig. 1). At the surface, steam seeps among recent lava flows have issued forth from these features.

The eruptive fissures according to Moore and Krivoy (1964) mark the intersection of the surface with a fault plane. Furthermore, Moore and Richter (1962) and Moore and Krivoy (1964) suggest that the regularity in placement of the vents, craters and scarps delineate not only the surface expression of the rift but possibly a subsurface southward dip as well. The example of these relationships discussed by Moore and Krivoy (1964) is the Hilina fault system which they believe is a gravity fault intersecting the main rift system at depth. Swanson et al. (1976) agree that gravity faults characterize the Hilina fault system but hypothesize that these features are secondary and point out a region south of the rift and north of the Hilina fault system that is unfaulted (Fig. 1).

A major fault zone was hypothesized by Ryall and Bennett (1968) based on the interpretation of a seismic refraction profile through Kilauea. This fault zone was proposed to extend through Kilauea caldera and dip towards the northeast. In this scheme, uplift occurred southwest of the caldera and subsidence to the northeast. The nature of this faulting would be largely subsurface as there is no surface evidence to support this type of faulting along the east rift (Macdonald, personal communication, 1977).

Below the surface, the rift is believed to be an arrangement of dense nearly vertical dikes, each dike about 2 meters wide (Macdonald, 1956). The vertical extent of the dikes in the rift system is unknown as pointed out by Fiske and Jackson (1972) but Macdonald (1956) suggested that the dikes reached the level of the magma reservoir of the summit region, about 2-4 km below the surface.

The nature of the gravity anomaly over the east rift may provide some clues as to the shape of the intrusive complex. The asymmetric shape of the gravity anomaly on the east rift with steeper gradients on the south side is the result of a wedge shaped prism with a gentle sloping north face and a steep sloping south face according to Swanson et al. (1976). The prism would be the expected result of southward growth of the rift as the younger dikes intrude on top of the older dikes to the north. As the younger dikes intrude at higher elevations, the rift would grow southward and upward.

One of the questions that we hoped that the 1977 refraction survey might answer was concerning the orientation of the intrusive structure at depth. Does the intrusive body dip? And, if so, in what directions? The orientation of the intrusive complex might shed some light on the present development of the rift.

In addition to investigating the nature of the intrusive body, other aspects of the crustal structure that we expected to study included:

- (1) The nature and relationships of the surface expression of the gravity and magnetic anomalies.

- (2) The lateral extent of the rift and its subsurface conformity to the regional crustal structure.
- (3) The velocity structure of the crust from seismic refraction analysis as compared to the velocity structure of the core samples from the geothermal well site (Fig. 2, pt. A).

In addition to a description of the various refraction, gravity and magnetic surveys and their interpretation, there are also sections of this thesis summarizing the results of the microearthquake and petrological studies.

PREVIOUS INVESTIGATIONS

Previous refraction studies of the island of Hawaii involved either long refraction lines with shot-receiver separations of two kilometers or more (Ryall and Bennett, 1968; Hill, 1969) or short refraction lines with shot-receiver separations of generally less than 2 km (Suyenaga, 1976).

Based on a partly reversed seismic refraction profile conducted onshore from Hilo to Kalae (Fig. 1), Ryall and Bennett (1968) indicated that the crust on the northeast coast of Hawaii in the vicinity of Kilauea could be separated into three layers (Fig. 10):

- (1) A basal layer from 6-7 km thick with P-wave velocities of 7.0 km/sec corresponding to the principal volcanic layer of the crust.
- (2) A second layer with a velocity of 5.3 km/sec and less regular thickness.
- (3) An upper layer varying in thickness from 1.2-2.5 km and represented by P-wave velocities of 3.0 km/sec. This layer is believed to be a series of fractured vesicular lava flows.

Ryall and Bennett (1968) also concluded that the southeastern flank including Kilauea volcano is being uplifted and inflated by magmatic intrusions. This interpretation was based on an offset in travel-time data in the Hilo-Kalae refraction profile which was believed to represent a fault zone.

In Hill's (1969) refraction study shots were fired every 10 km offshore with recording onshore spaced at 25 km intervals. Additional recording was covered by the seismographic stations maintained by the U. S. Geological Survey's Hawaii Volcano Observatory.

The results of this study suggested that the crust under Hawaii can be separated into two principal layers (Fig. 10).

- (1) A basal layer from 4-8 km thick with P-wave velocities of 7.0-7.2 km/sec.
- (2) An upper layer from 4-8 km thick with P-wave velocities of 1.8-3.3 km/sec at the surface to 5.1-6.0 km/sec at depth.

Hill (1969) speculated that the basal layer was probably the old oceanic crust under Hawaii including the intrusives associated with the vents and rift zones and the upper layer probably consisted of lava flows forming the bulk of the crust.

It was also noted by Hill (1969) that the early P-wave arrivals from the summits and major rift zones of the volcanoes are indicative of material of velocities up to 7.0 km/sec approaching the surface to within 2 or 3 km.

Suyenaga (1976) recorded two refraction lines, one across the rift and the other just off the rift. Along each line, six shots were fired ranging in size from four to sixteen pounds. The shots could be detected at distances of 2-3 km.

Beneath the surface layer, velocities of 2.5 km/sec and 2.9 km/sec were observed on the flank and 3.1 km/sec over the rift, Fig. 10 (Suyenaga, 1976). The experiment did not succeed in determining the depth to which velocities higher than 3.1 km/sec were observed.

FIELD DATA

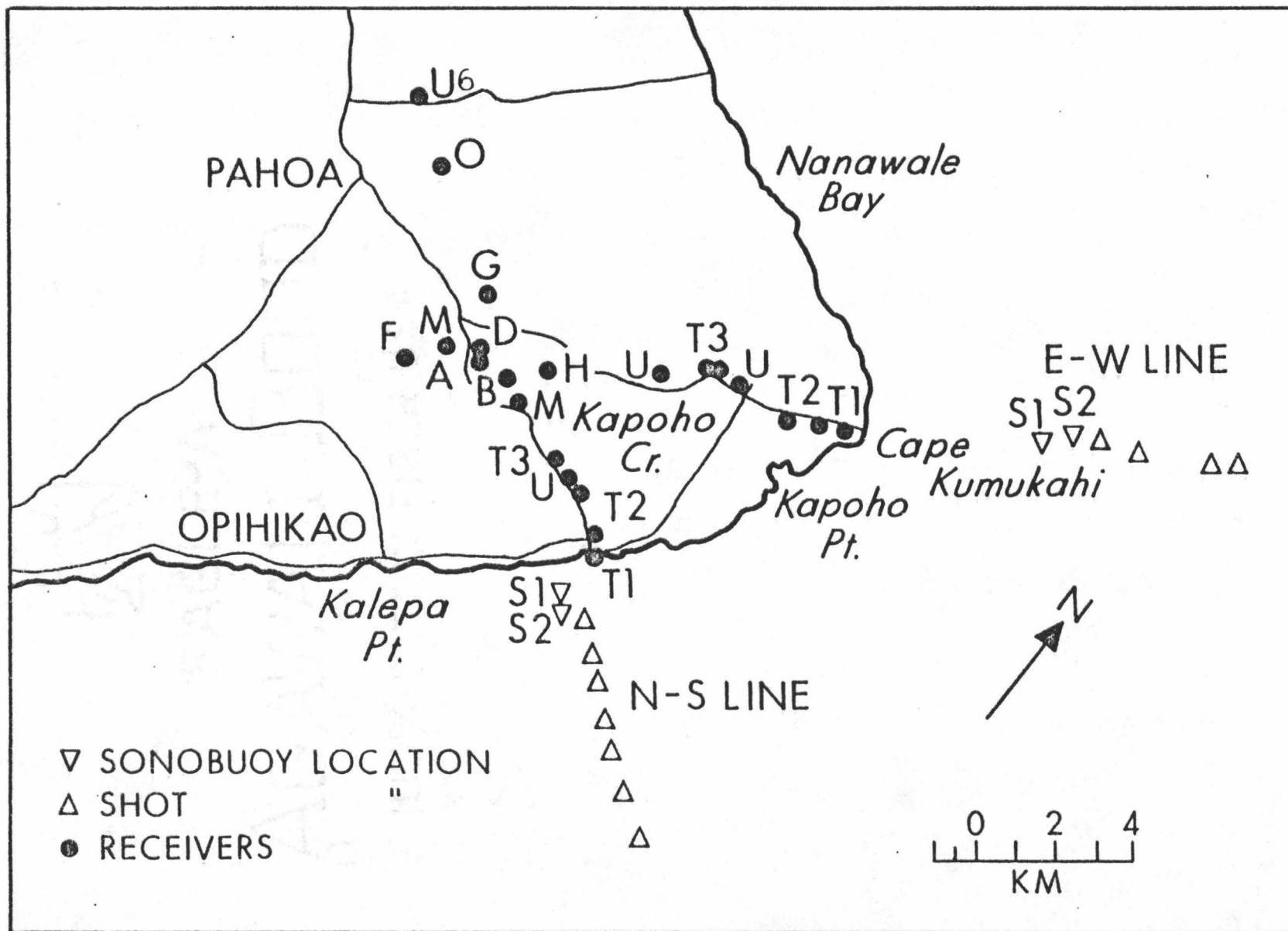
Two refraction lines were completed in Puna, Hawaii in January 1977. One line, the EW line, spanned some 22 km along the strike of the east rift from south of Pahoa through the geothermal well site (Fig. 2, pt. A) to Cape Kumukahi. The other line, the NS line, stretched 12 km from north of Pahoa to the coast (Fig. 2).

Various types of seismometers were deployed along these lines. The Hawaii Institute of Geophysics manned stations (Fig. 2, pts. T) consisted of a 4 channel R-70 type TEAC cassette recorder connected to a AS-110 Sprengnether amplifier on two to three seismic channels. The fourth channel on the TEAC was used to monitor WWVH radio time signals with on-station voice announcements. The TEAC's used 30-60 minute tape cassettes turned on a few minutes before each shot and off when there was a delay in the shooting schedule.

The University of Texas at Dallas systems (Fig. 2, pts. U) used a self-contained reel-reel magnetic tape recorder set on a 10 day cycle. The system contained both a WWVH receiver and an auxiliary time code generator synchronized with a traveling clock. The geophone was connected to the recording drum with a 20 foot cable.

At one location on both the NS and EW lines, a Sprengnether microearthquake system (Fig. 2, pts. M) was connected to a Hall-Sears 1 Hz geophone. Smoked paper was used and changed at the end of each day's recording.

Figure 2. Puna, Hawaii showing positions of the shots,
receivers, and sonobuoys used in the 1977
refraction survey.



Around the well sites at locations A, B, C, D, F, G and H were located the array network. The array utilized Mark Products L-25, 4.5 Hz geophones. Three of the elements A, F and G were telemetered on frequencies of 162-166 MHz from the positions indicated (Fig. 2). The other elements of the array as well as the TEAC geophones were hardwired with disposable type torpedo wire placed on the surface with distances of up to 1 km.

The signals from the telemetered and hardwired geophones were amplified by twelve channel system that multiplexed the signals into two channels of a tape recorder. This system was developed by the Hawaii Institute of Geophysics (H.I.G.) geothermal group. The tape recorder used was a Hewlett-Packard reel-reel type unit located at a temporary field communications center.

Three ocean bottom seismometers (OBS) were borrowed from the marine geology group at H.I.G. and were used unmodified. The basic units were buried just below the ground at six locations on the EW and NS lines after being placed on a 15 day recording time speed back at the laboratory. Two of the three units did not function properly due to problems with the tape cassette system. The third OBS revealed a large error in timing in its tape recording system (Fig. 2, pt. 0). The error was large, varying from one to two seconds and the data were not used in the analysis. One possible source of error may have been from thermal effects as the instruments experienced significant temperature changes from day to night while near the surface.

After the recording instruments were properly deployed and ready, the 60 foot vessel Noi'i commenced to fire shots outward from the coast along both the EW and NS lines (Fig. 2). The charges were alternately detonated in 60 and 120 lb sizes. All shooting was performed at night starting at eleven pm on the evening of June 13 and 14, 1977. It was felt that a night shooting schedule would encounter a minimum of noise and attention as shots were fired only a few kilometers offshore.

To improve the positioning of each shot, a sonobuoy was deployed about 1 km offshore on both lines. The sonobuoy was equipped with a transmitter and relayed the water wave arrival time at the sonobuoy to the nearest onshore stations (T1 and T2, Fig. 2). Surveyor's transits were positioned at two points on either side of stations T1 and T2 for locating both the sonobuoy and shots. Upon commencement of the shooting each night, the sonobuoys were picked up and fixes were taken again to determine the drift. An attempt was made to anchor the sonobuoy but the water was very deep and the anchor evidently did not reach the bottom. As a result, there was some drift of the buoy during the course of the shooting (Fig. 2).

During the shooting schedule, communications varied from good to poor depending upon the location of the various mobile parties. The high antennas of the array generally provided for communications with the boat but the nature of the terrain at the various seismometer sites caused intermittent reception of the mobile parties with the boat. Although communication was a problem at times,

everyone knew when to turn on their recording instrument as a 30-45 minute shooting window was decided upon beforehand. Within this shooting window, shots were scheduled to be fired every five minutes.

The time signal that was recorded on all of the instruments was the radio transmitted WWV from Maui, Hawaii. To prevent interference at critical moments during the recording, auxiliary timers such as traveling clocks or other standby radios tuned to other frequencies of WWV helped to remedy this hazard.

DATA REDUCTION AND ANALYSIS

Refraction data from the TEAC cassette recorder and Hewlett Packard recorder were played back on a six channel visicorder as well as a two channel pen-recorder.

Interference and poor reception over WWVH radio obscured some of the time marks on the tapes. For these records, the time signals were passed through a band filter centered at 900-1100 HZ to reduce the background noise as much as possible. In some places on the tapes, the time signal was so poor that an auxiliary time mark from a TS-250 timer was synchronized with an oscilloscope showing a second tick somewhere prior to the shot record. This bootstrap operation was subject to a reaction time error of 1/10-1/20 second as it involved manually synchronizing the second marks.

Accurately positioning the shots on the EW line presented additional problems. Possible local magnetic variations as well as binding in the needle of the compass in one of the surveyor's transits centered at the T1 location has led to some of the original transit data being reworked. An additional factor was that the transits were close together compared with the shot positions offshore; this meant that a small difference in angular displacement might give rise to errors in offshore positioning. All the transit data were therefore checked with respect to the recorded landmarks. The shot positions on the EW line appear to be more irregular and further apart than on the NS line with fog preventing the sighting of shots 1, 6, and 7.

As a check on the sonobuoy position, the T-phase was subtracted from the P-wave arrival for each shot at the TEAC 1 site and then multiplied by the velocity of water, 1.50 km/sec (Matthews, 1939). This procedure gave distances very close to those measured by the transits for the two sonobuoy positions and additional indication that the transit data were reasonable (Fig. 3).

It was discovered that the sonobuoy drifted during the course of the experiment. The apparent drift was from S1 to S2 on the map, Figure 2 (note the apparent larger drift on the EW line). The assumption was made that the sonobuoy drift was linear as transit sightings were taken only just before and just after sonobuoy deployment and recovery.

To check the validity of the assumption of linear drift for the sonobuoy, the T-phase arrival times were compared to the sonobuoy arrival times for the NS and EW lines (Figs. 4 and 5). The results for the NS and EW lines seem to indicate that there was a significant amount of drift of the sonobuoy positioned on the EW line as compared to the sonobuoy on the NS line. Another way of looking at this is, that the increasing time between the sonobuoy and T-phase arrival for the EW line (Fig. 5) appears to be due to an increasing distance between the sonobuoy to shot. This increase of distance appears to be explained by the sonobuoy's drift away from its initial deployment position. Thus the sonobuoy's position at any given shot may be determined by subtracting the P-wave

Figure 3. Seismograms centered on the P-arrival. The T-phase and sonobuoy arrivals are also visible.

N-S LINE TEAC 1 SEISMOGRAMS SHOWING P, T AND SONOBUOY ARRIVALS

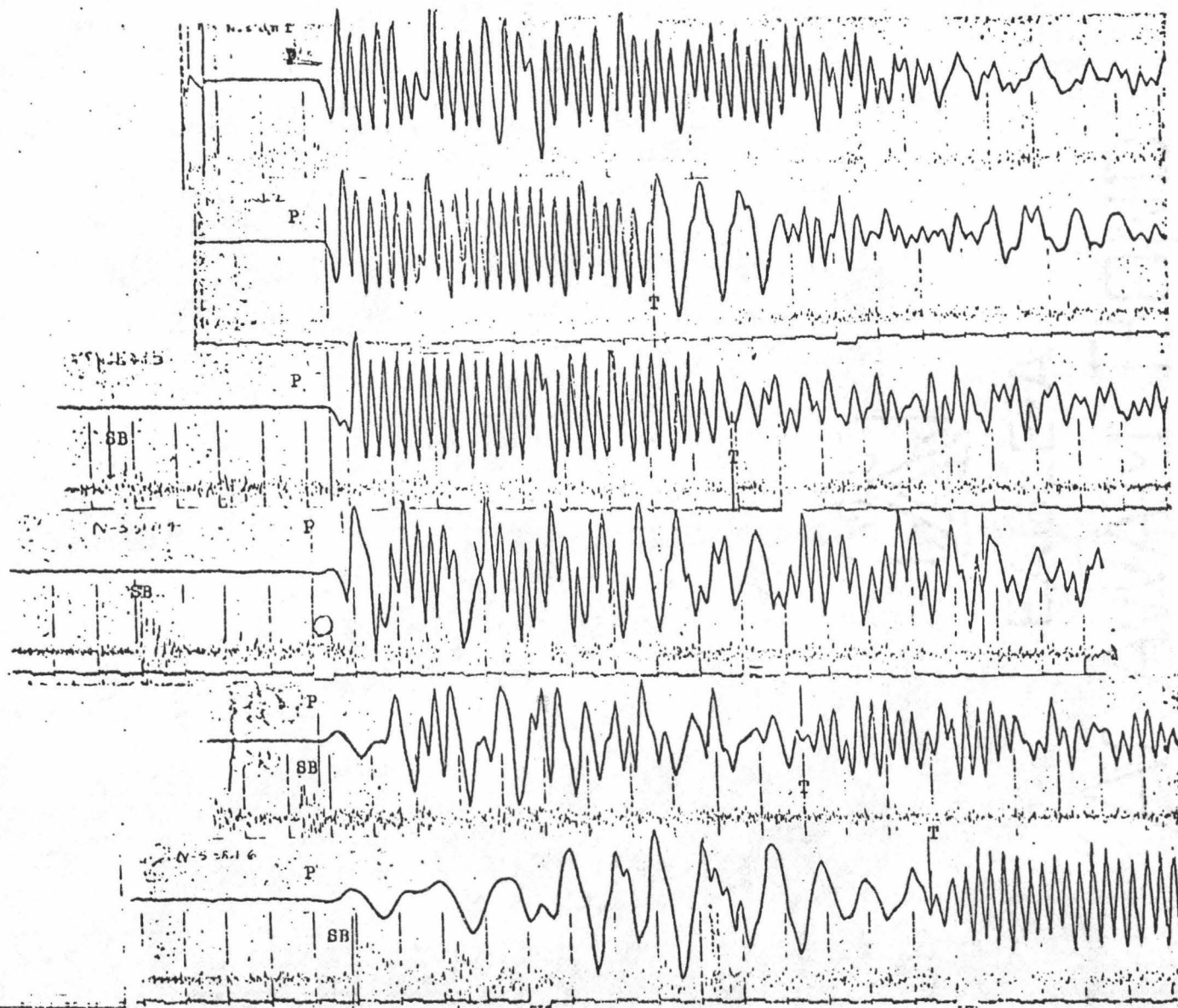


Figure 4. The NS TEAC 1 (T1) seismogram arrival times of the sonobuoy and T-phases for shots 2-7.

N-S LINE. SONOBUOY AND T-PHASE ARRIVAL TIMES FOR SHOTS 2-7

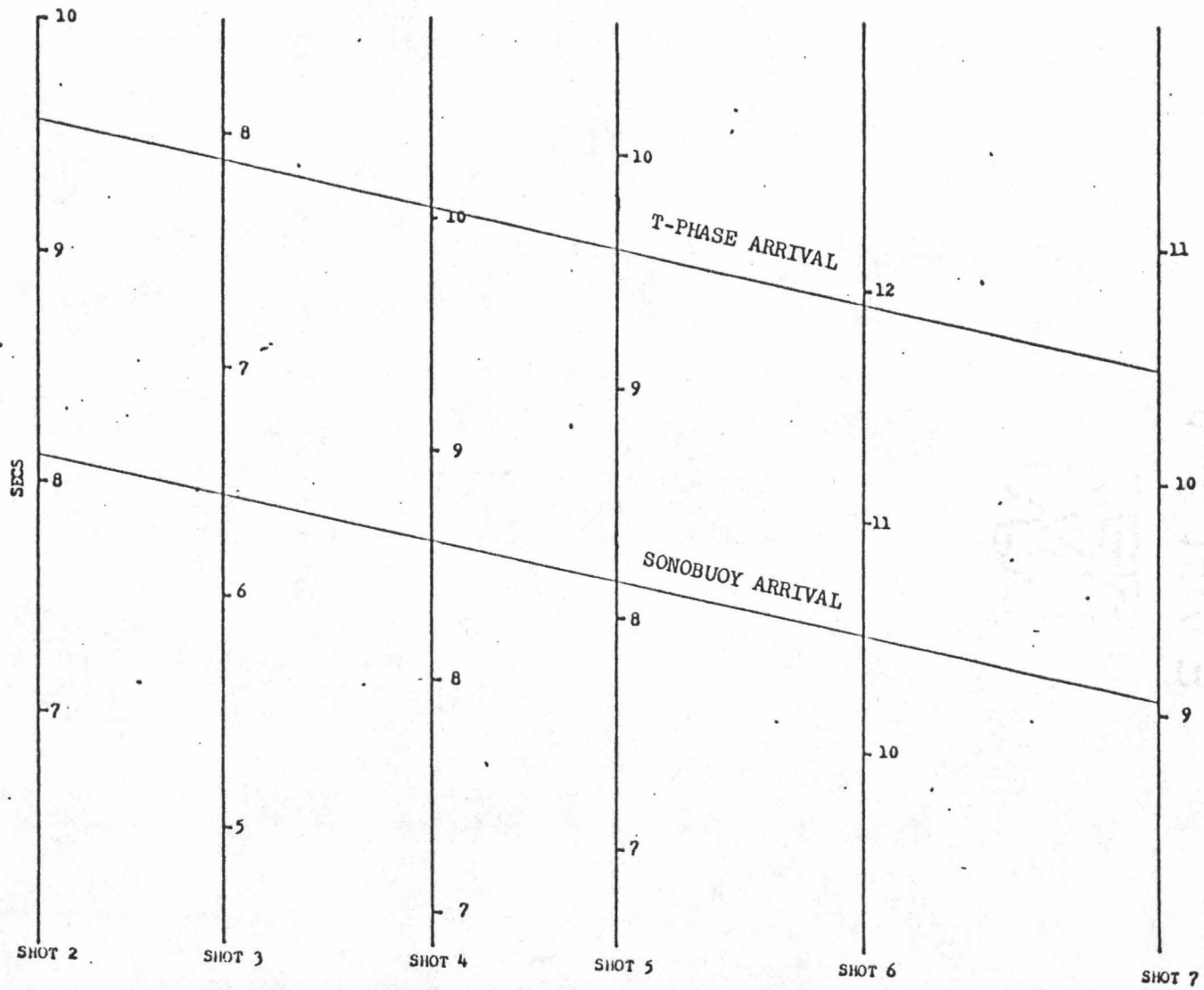
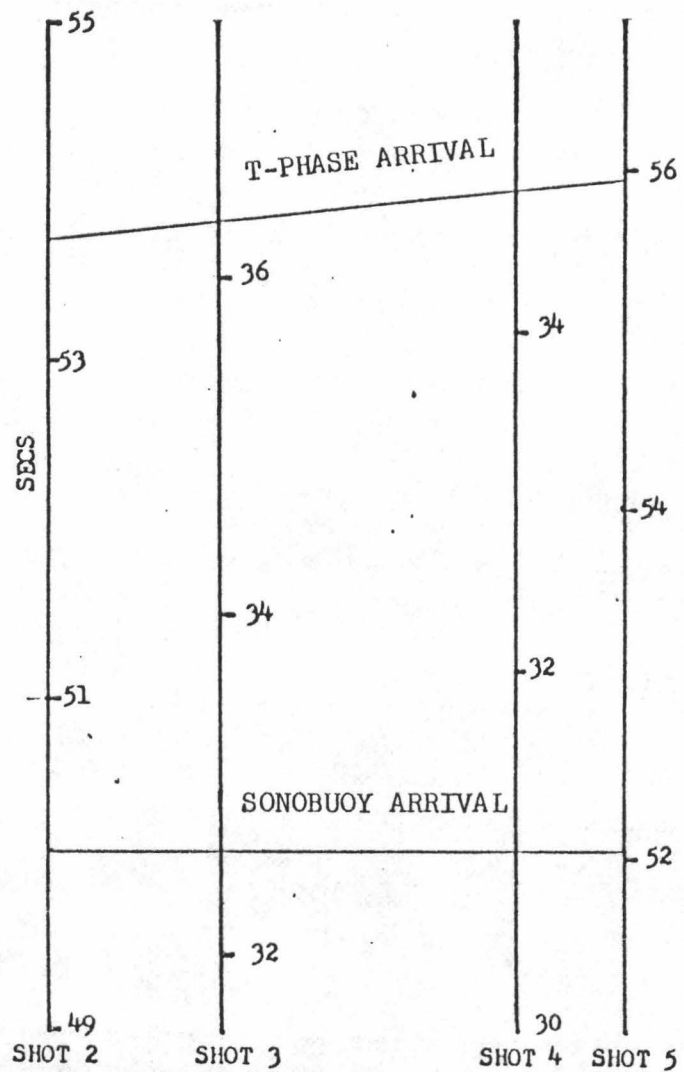


Figure 5. The EW TEAC 1 (T1) seismogram arrival times of the sonobuoy and T-phases for shots 2-7.

E-W LINE. SONOBUOY AND T-PHASE ARRIVAL TIMES FOR SHOTS 2-5



arrival from the T-wave arrival and multiplying by the velocity of water.

In order to obtain a shot instance or origin time for each shot on the EW line the approximate distances from the sonobuoy to each shot were used as discussed above. The shot instance was obtained by subtracting the (sonobuoy distance to each shot)/(velocity of water) from the sonobuoy arrival time broadcast to the TEAC 1 site. The shot instance was subtracted from the local WWVH receiver time giving the travel time from the shot to the various receivers.

On the NS line boat records there were second ticks distinguishable up through shot 5, although the second ticks were unmarked. Since the second ticks were unmarked, this necessitated making an estimate to the nearest second by taking the ratio, (shot distance/velocity of water) as the total number of seconds for the water wave to travel that distance. Thus, the origin times for most of the NS shots could be determined directly as these records also recorded the explosion arrival time.

The next correction was for water depth or bathymetry. The boat did not measure the water depths continuously throughout the shooting but only upon deployment of the sonobuoy. To measure the approximate depths along each shot line the boat's course was plotted on a bathymetric chart of Hawaii (C.G.S. 4115) as well as a chart based on a study by Malahoff and McCoy (1967). Approximate depths were measured for each shot for both lines with bottom contours indicating a steep offshore slope, varying from 15-21 degrees along the NS shot line (Fig. 6).

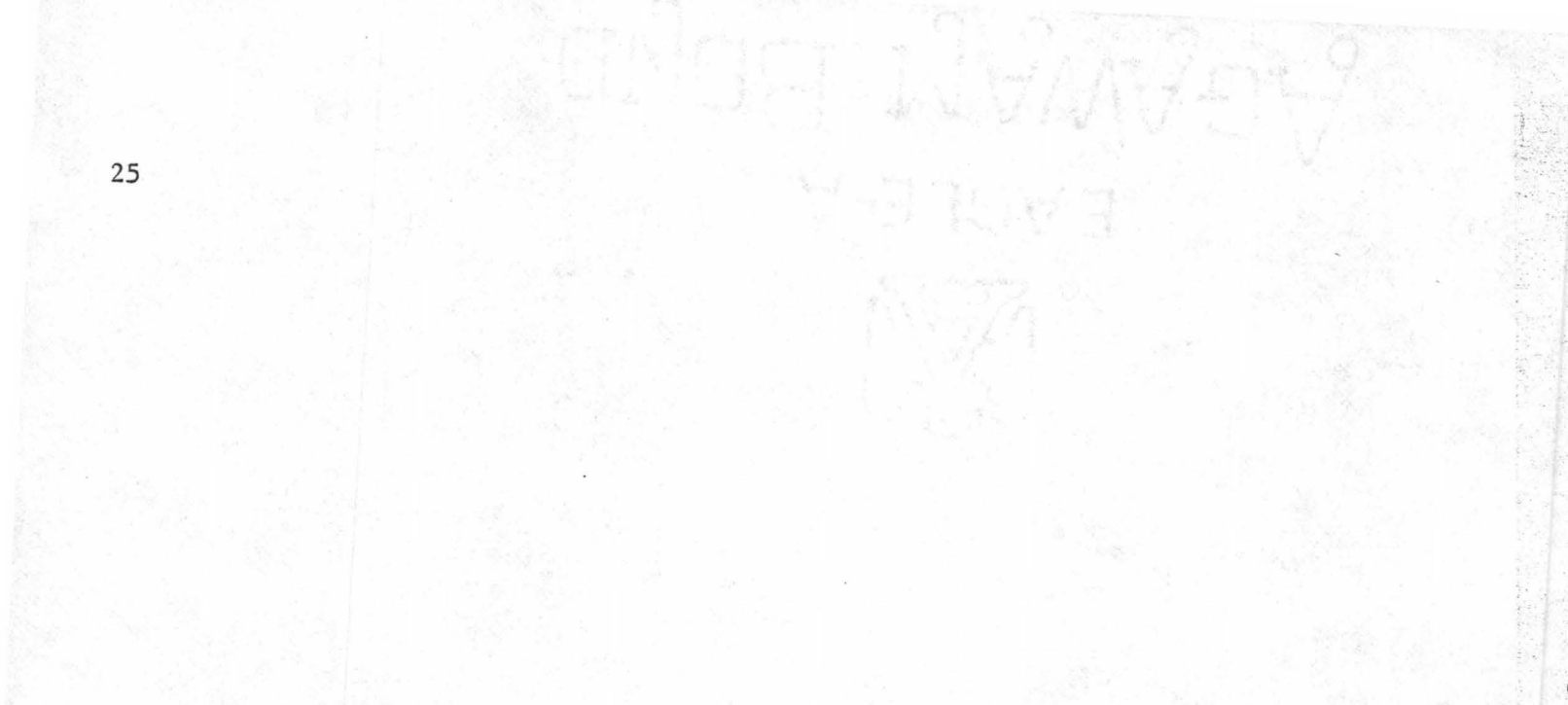
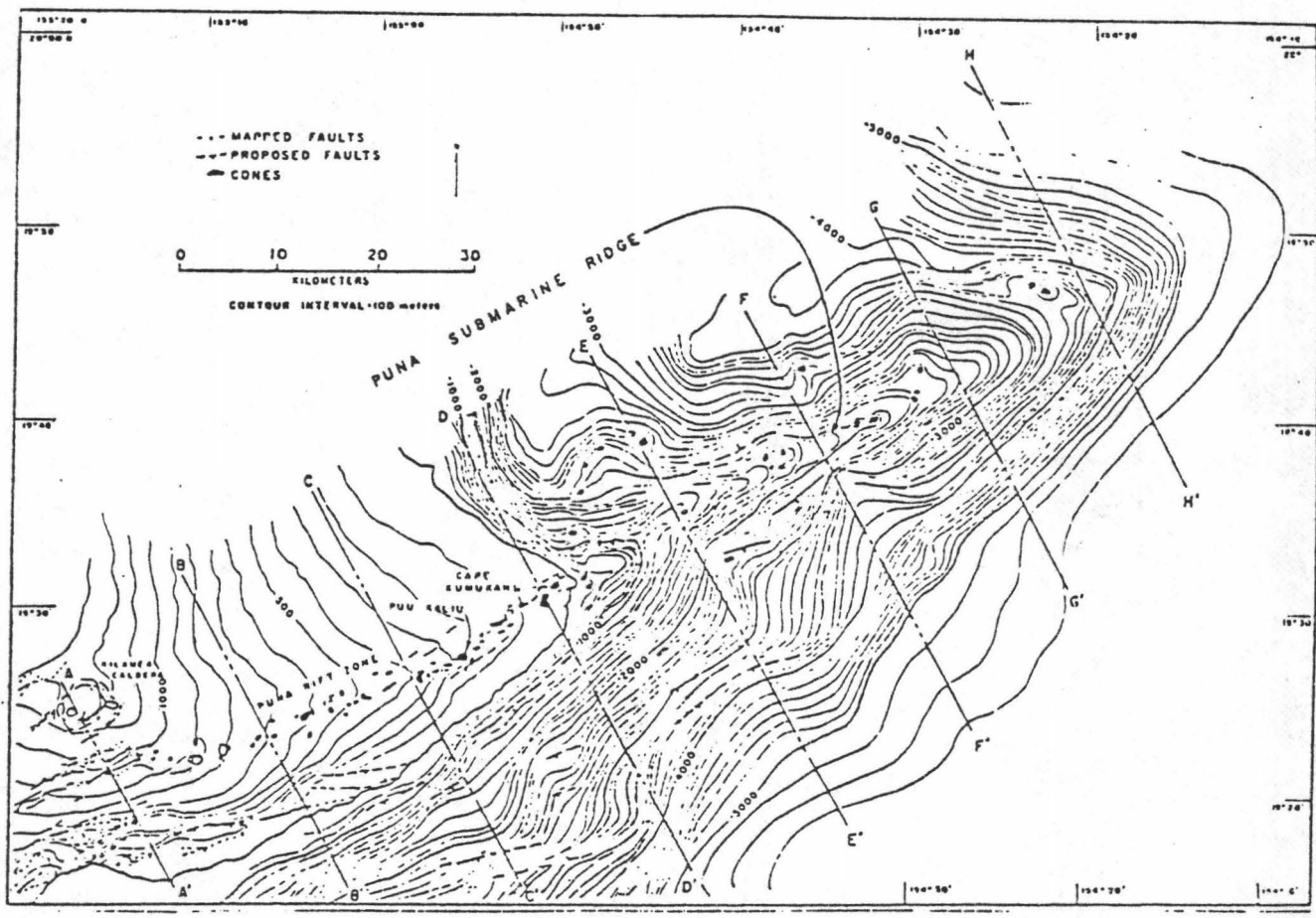


Figure 6. Bathymetry, geological features and topography of the Puna rift zone and the Puna submarine ridge from Malahoff and McCoy (1967).



Using a water velocity of 1.5 km/sec for this area (Matthews, 1939) and an upper layer velocity of 2.8 km/sec (this average velocity was assumed from Suyenaga's (1976) refraction study), delay times were calculated for the shots and refracting horizons using the principles as outlined by Nettleton (1939) and Dobrin (1960). These delay times were subtracted from the elevation corrected shot times to arrive at the travel times through the datum plane at sea level. The intercept times differences varied from 0.10-0.20 secs for the travel-time plots of the same refractor velocities (Figs. 7 and 8). Those were, however, larger differences in intercept times for some of the shots; this will be discussed in the next section.

The following are possible sources of error in the water depth corrections.

- (1) The uncertainty in the water depths along the EW shot line was estimated to be ± 200 m and ± 100 m along the NS line as depths were taken from the only available sources, large scale navigation charts. Calculations show that for an uncertainty of ± 100 -200 m, correction errors for water depths would be from 0.1-0.2 second.
- (2) The datum plane corrections for water depths were based on using overlying layers of velocity 1.5 and 2.8 km/sec. There may have been other layers between the surface and the high velocity layers of 5.7-7.0 km/sec that were not observed in the data.

Travel time plots were constructed after subtracting the elevation corrections of a given receiver assuming a sea level datum plane. The elevation corrections ranged from 0.0-0.3 secs using the upper layer velocities as discussed above. Two types of travel-time plots were used:

- (1) a given shot vs the station position or "array plots".
- (2) a given station vs shots 1-7 or 2-5 or "station-shot plots".

The EW data were also plotted up centering shots 2-5 at the TEAC 1 site and recomputing the respective receiver positions from this point. This procedure gave the velocities across the array and provided a method of checking the velocities obtained from the standard type of travel-time plot. The refractor velocities from this method were in agreement with those velocities determined from the standard travel-time plots.

In calculating the crustal structure, flat lying layers of homogeneous composition were assumed (Nettleton, 1939; Dobrin, 1960) along with the velocities and structures of prior surveys in the region (Ryall and Bennett, 1968; Hill, 1969; Suyenaga, 1976).

On the NS line, depths were calculated using the critical distance technique as well as the time intercept method (as an upper layer of 3.0 km/sec was observed on three of these plots). Both of these techniques yielded similar results.

On the EW line, there were no visible breaks seen from the low to high velocity material. In this case, an upper layer of 3.0 km/sec was assumed and the depths were calculated on the basis of critical distances and intercept times.

SEISMIC REFRACTION RESULTS

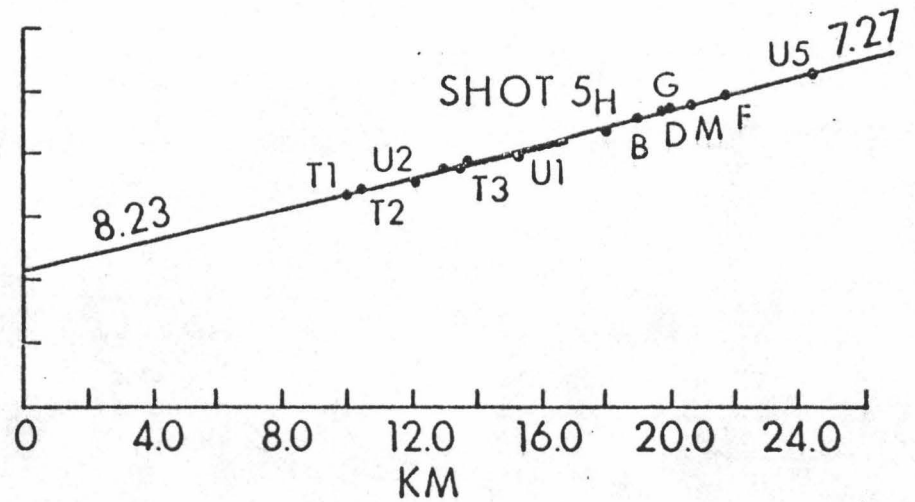
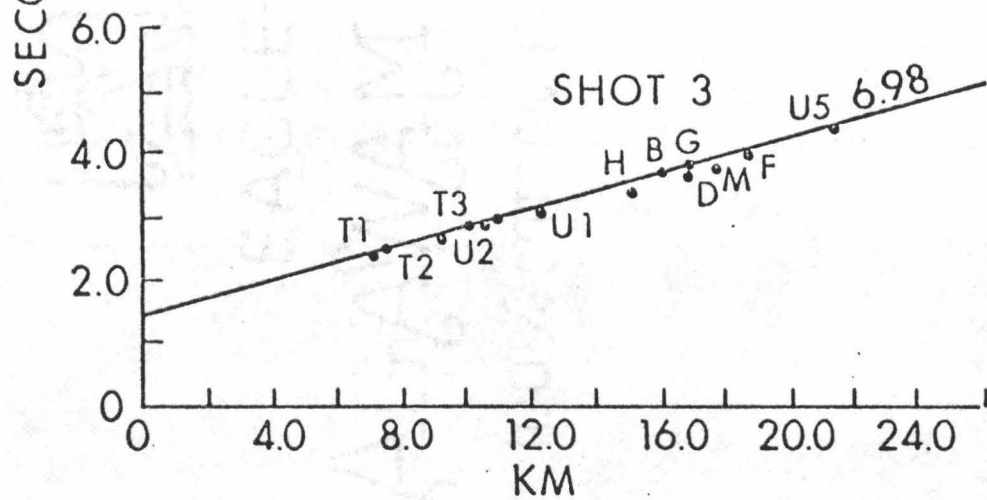
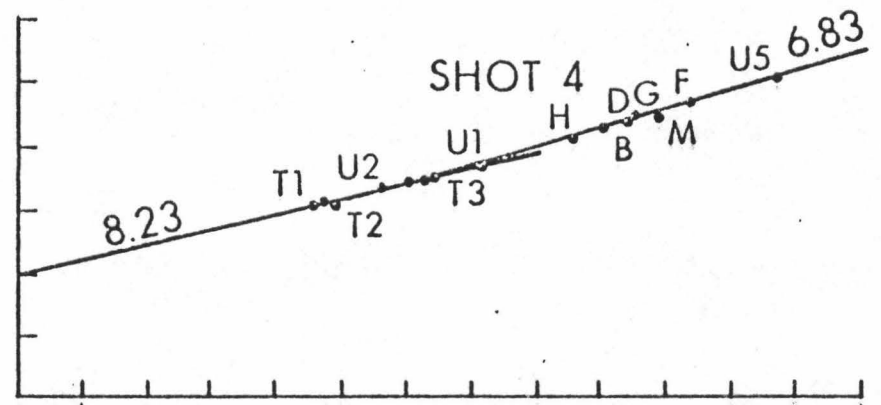
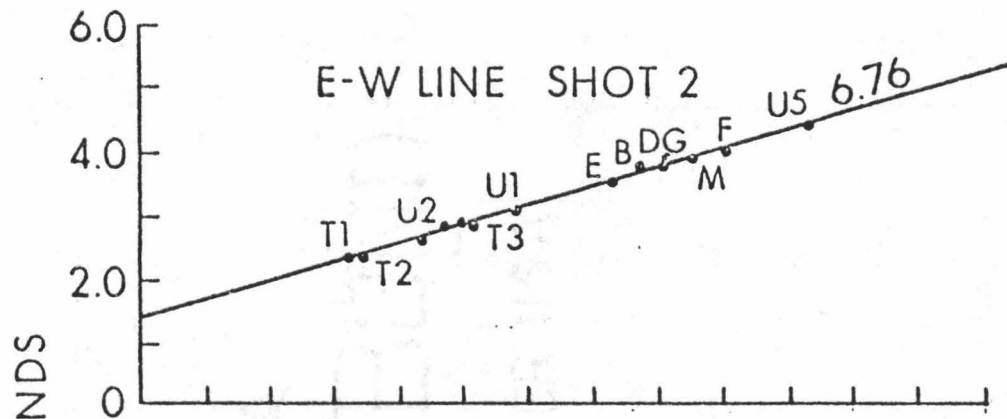
The seismic refraction data corrected for both elevation and water depths as described earlier were next subjected to analysis using standard travel-time plots. The first type of plot, the array plot (Figs. 7 and 8), shows a given shot vs the various receiving stations. This type of plot was constructed by scaling the distances from the various receiving stations to the shot point against the corresponding travel time. The advantages of using this type of travel time plot are:

- (1) variations in time from one shot to the next are eliminated as just one shot is plotted at a time.
- (2) the structure deduced from this type of plot is indicative of the structure directly beneath the station.

For the second type of plot, data were plotted in the form of station-shot configurations. In this case a station, for example T1 (Fig. 9) is scaled against the corresponding positions and times of the shots on the line. If the origin time of the shots was not precisely determined, as was the case for some shots in this survey, one might expect to see large variations in the data on this type of graph.

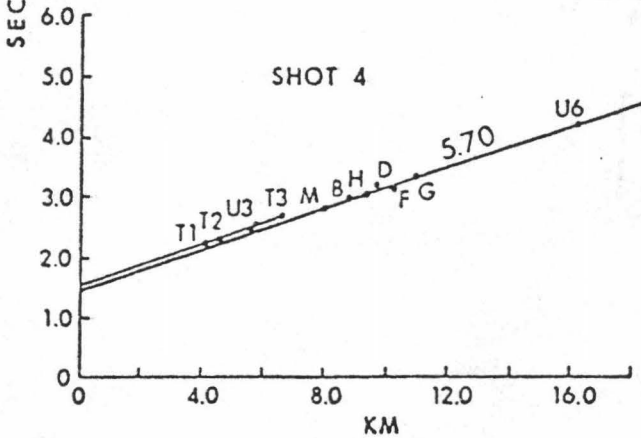
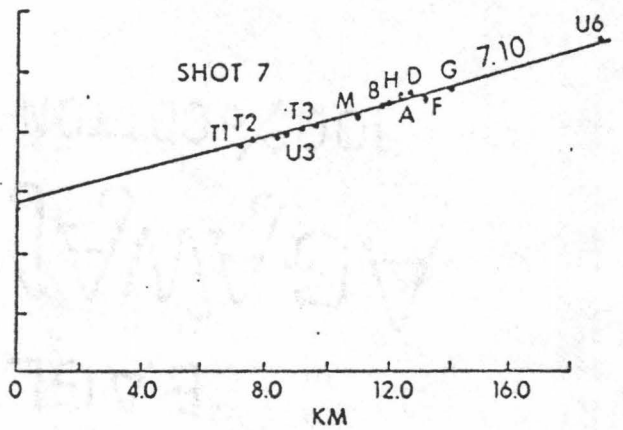
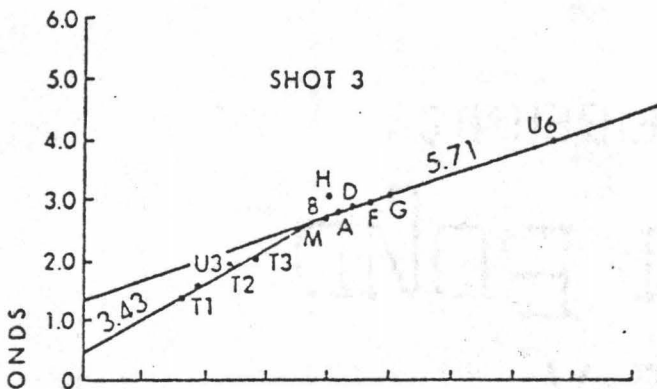
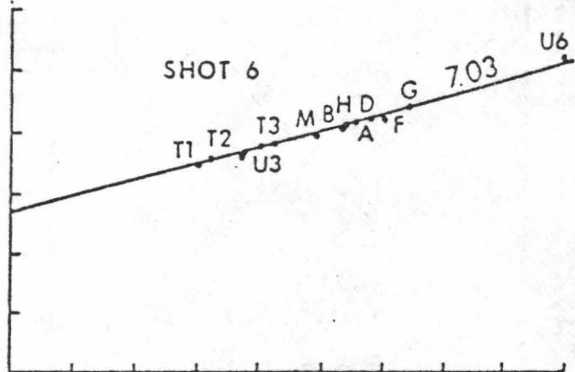
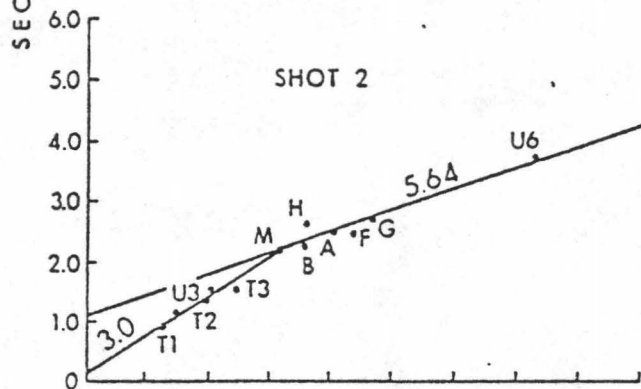
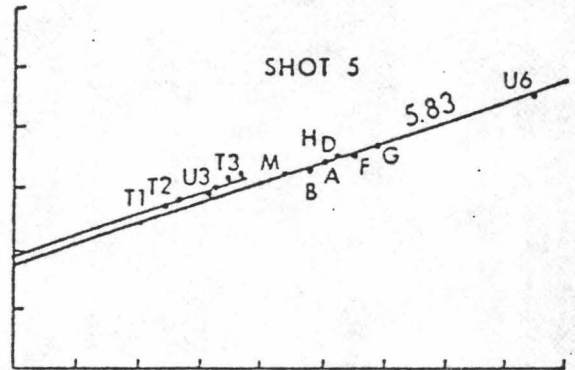
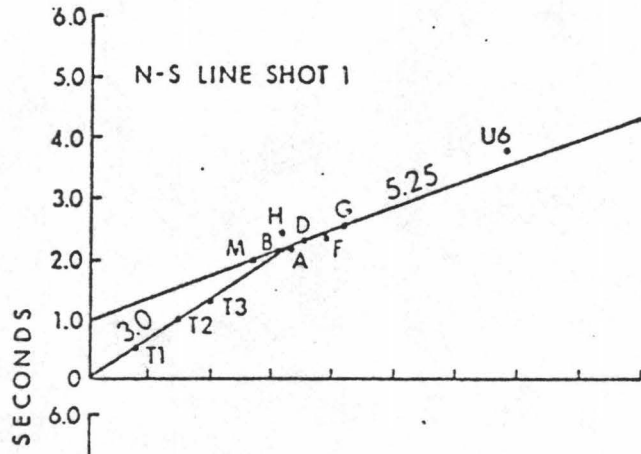
A description of the various travel-time plots included in this section will now follow and refer to Figures 7-9. First the travel-time data for the EW line will be discussed.

Figure 7. The travel time plots for the EW line shots 2-5.



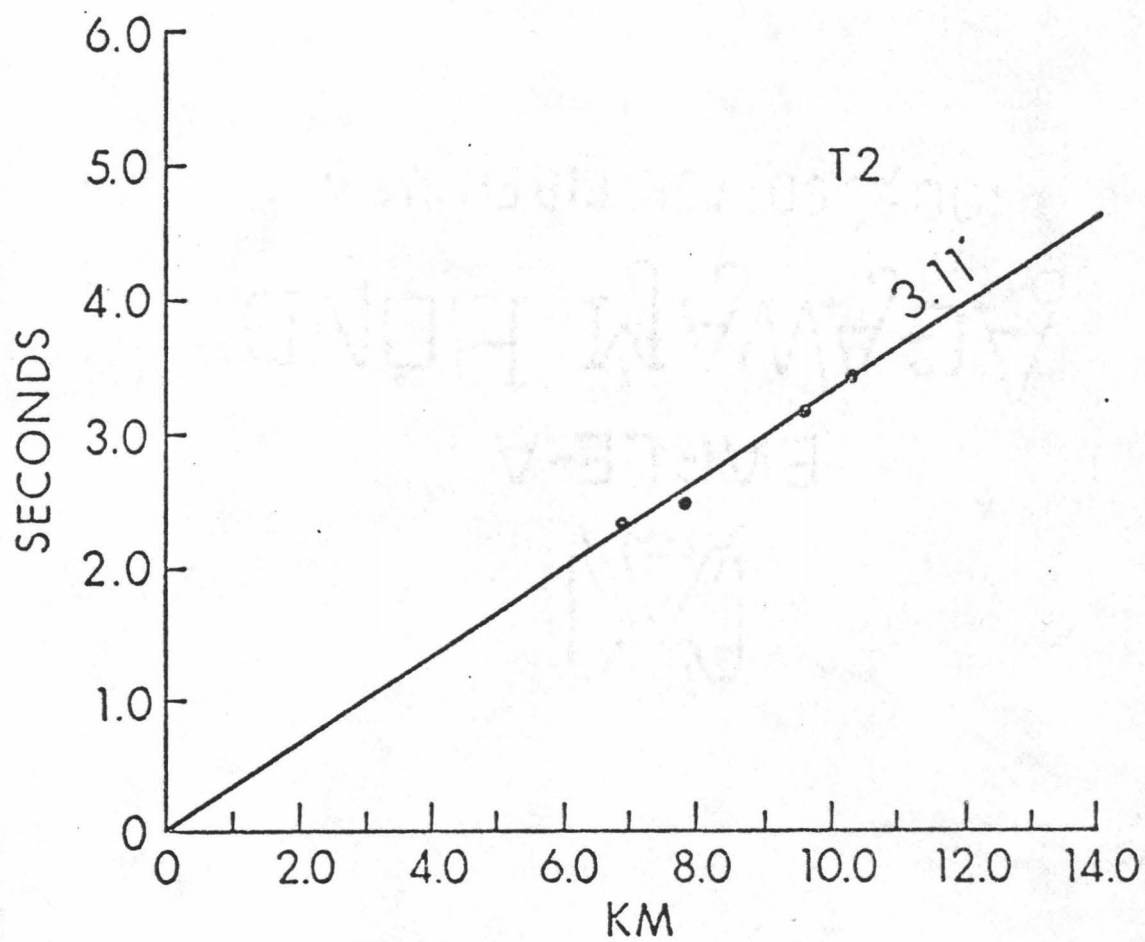
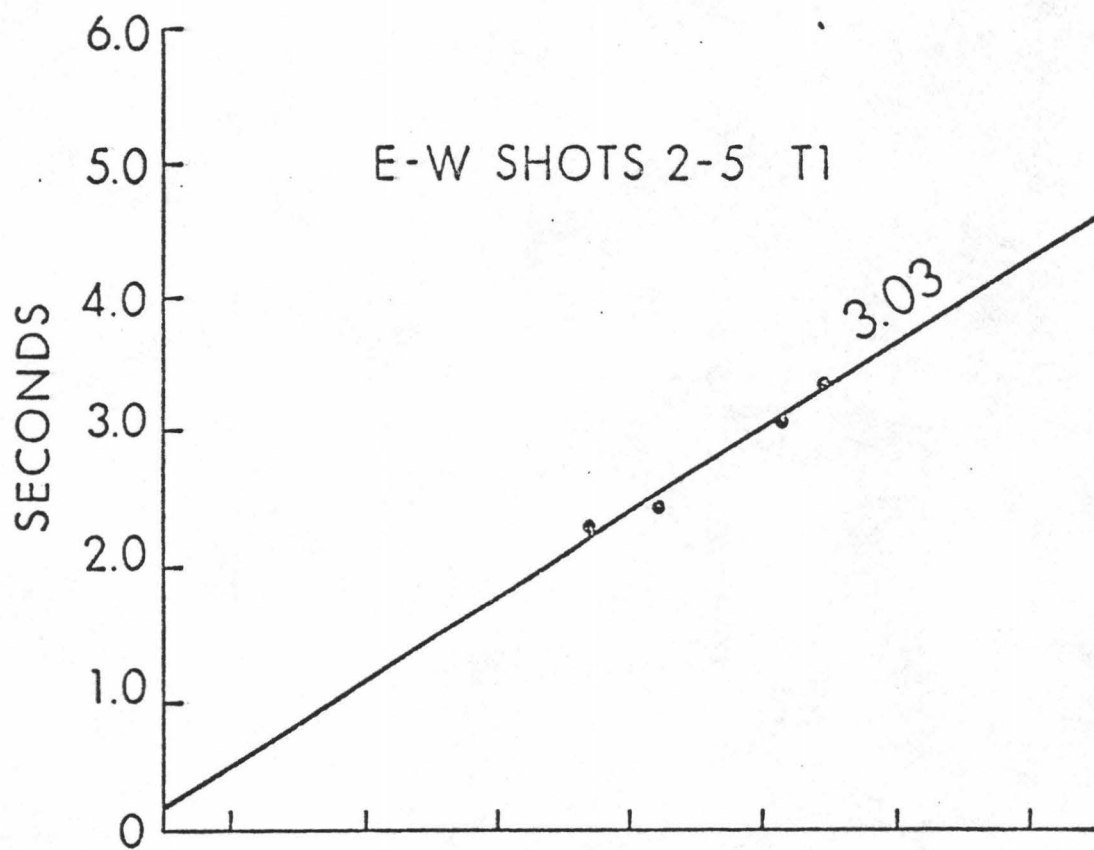
AGAWAM BOND
EAST
PA

Figure 8. The travel-time plots for the NS line shots 1-7.



]

Figure 9. The travel-time plots for the EW line TEAC 1 and TEAC 2 (T1 and T2) locations, shots 2-5.



The travel-time data for EW shot 2 show a velocity of 6.76 km/sec across the entire array with all time variations less than 1/10 sec. There were no other velocities observed on this plot.

The travel-time data for EW shot 3 indicates a velocity of 6.98 km/sec for all receiving stations across the array with most time variations less than 1/10 sec. Notice that the travel time intercepts are about the same for both EW shots 2 and 3 at 1.4 seconds and this indicates that we are seeing the same layer.

Shots 4 and 5 have an anomalously high velocity of 8.23 km/sec through the first five stations followed by a return to velocities of 6.83 km/sec and 7.27 km/sec, respectively. All but a few data points fall within 1/10 of a second of the estimated velocity. The high velocity of 8.23 km/sec indicates that we are encountering some sort of structural anomaly in the Kapoho region (Fig. 2). However, the EW line is not reversed and it is not certain whether this anomaly is due to high velocity rock near the surface or anomalously dipping rock horizons.

Next, a brief description will be made of the travel-time plots for the NS line (Fig. 8). The NS line travel-time data for shots 1-3 are very similar in that they show two refractors, an upper velocity of 3.0 km/sec and a second layer velocity of 5.25-5.71 km/sec. The travel time intercepts are also very close.

The travel-time data for shots 4 and 5 are also similar in that they show not only apparent layer velocities and time intercepts that are very close (5.70 and 5.83 km/sec) but also exhibit a curious

offset in the travel time amounting to 0.1-0.2 seconds. This effect might be the result of a fault line displacement but we cannot be sure as this line is unreversed.

Shots 6 and 7 exhibit the same trends as the other two groups of shots. The velocities are very close, 7.03 and 7.10 km/sec and the time intercepts are just under 3 seconds each. All but a few data points fall to within 1/10 of a second of the best estimated velocity for all the data.

In summary, on the NS line travel-time plots, the following velocities are observed; 3.0 km/sec, 5.25-5.83 km/sec and 7.0-7.1 km/sec (Fig. 8). Upon examination of these plots, one can observe that there are no shooting configurations or travel-time data that show all three apparent velocities (3.0, 5.7 and 7.0 km/sec) occurring together on the same travel-time plot. It should also be apparent from these travel-time graphs that we are handicapped by a lack of data points between the array stations and remote recording station U6 (Figs. 2 and 8). One cannot be certain, therefore, of the relationship of the 5.7 km/sec (apparent average velocity of the 2nd layer) refractor to the 7.0 km/sec refractor across the rift.

The apparent average velocity of 5.7 km/sec from the NS line is not observed on the EW travel-time plots and some possible reasons for this are:

- (1) the 5.7 km/sec layer may thin out along the strike of the rift in the EW direction and may be too thin to observe in our receiver data for this line.

- (2) the 5.7 km/sec layer may lie principally within the hydrothermal zone surrounding the geothermal well site. This layer would be highly fractured and probably permeable causing a low velocity zone within the intrusive anomaly which is not observed in certain recording configurations.
- (3) the 5.7 km/sec velocity may be the result of the intrusive body dipping northwards at a 6-7 degree angle. From flat layer refraction analysis, we know that the velocity structure observed near a receiver will be true only if the effect of the dip or inclination of the rock layer is determined (Nettleton, 1939; Dobrin, 1960). If a refractor is dipping it will give an apparent velocity higher than the actual velocity if the structure dips upward from the shot path origin towards the receiver and lower than the actual velocity if the structure dips away from the receiver and upwards towards the shot point. To be sure of the actual dip, one would have to account for the ray paths on both sides or ends of the shooting-receiving profile. In this case, the NS line is only a single ended profile and we cannot be sure that the 5.7 km/sec average velocity observed is, in fact, the result of the 7.0 km/sec layer dipping towards the north. If, however, we assume that the 7.0 km/sec layer dips toward the north side of the rift at

$6\frac{1}{2}^{\circ}$ angle, then an apparent velocity of 5.7 km/sec would be the result. The 7.0 km/sec velocity was observed on both the EW and NS profiles and we assume that this velocity is true.

The third possibility as described above, therefore cannot be established by refraction data. However, the dipping structure as described above was tested by modeling around the observed gravity anomalies (next section).

Velocities less than 3.0 km/sec were not observed in the 1977 refraction survey. Other studies have resolved this upper structure somewhat. Suyenaga (1976) indicates that a surface layer of 0.7-1.6 km/sec extends from 100-300 meters deep and overlies layers of 2.5 and 2.9 km/sec (Fig. 10). Hill (1969) found a 3.1 km/sec layer extending regionally 2-3 km deep with a surface layer of 1.8 km/sec (Fig. 10). In our study, the values of the velocities and depths of the surface layers were borrowed from Suyenaga (1976) to make the elevation corrections to the sea level datum plane.

After all the velocities had been determined from the various travel-time plots, the structural arrangements and depths were calculated using the technique of flat layer formulas (Nettleton, 1939; Dobrin, 1960). From the EW line using the data from shots 2 and 3, the average of the depth determinations to the 7.0 km/sec horizon using both critical distances and intercept times and an overlying layer of 3.0 km/sec was found to be 2.5 km after 0.2 km were added to reduce the well site to sea level. Calculations were

performed using the data from the NS line as well. Assuming that the 5.7 km/sec layer is real, the depth to this layer would be from 1.6-1.8 km using the velocity-time relationships observed from shots 1-3 (Fig. 8).

The travel-time intercepts for shots 5, 6 and 7 on the NS line are at variance the refractors of about the same velocity on the EW line (Fig. 7 and 8). The travel-time plots for the NS line shots 6 and 7 indicate velocities of 7.0 and 7.1 km/sec, respectively. These velocities are closely matched to the corresponding velocities observed on the EW lines shot 2-5 and are presumably the same refracting horizon. The timing error as discussed earlier enters the picture here, and is responsible for delays of 0.5 sec for shot 5 and 1.0 sec for shot 7 on this line. As the timing error is responsible for this difference in the intercept timer, we cannot be certain of the exact magnitude and cause of this error other than it appears to increase with distance. On account of this error all structural calculations were determined from the shots closer to the shoreline on both the NS and EW lines (shots 2 and 3 on the EW line and shots 1-4 on the NS line).

From the array plots for shots 2-5 on the EW line and for the station-shot plots on the NS line, travel-time equations were derived (Table 1). These travel-time equations were used to derive the velocity-depth structure to be discussed.

The models derived from the travel-time data (Fig. 10) show a 3.0 km/sec layer overlying a 2nd layer of velocity 5.1-5.7 km/sec

which in turn rests atop of the intrusive anomaly of velocity 7.0 km/sec placed at just over 2 kilometers depth. Simple ray tracing along both the EW and NS lines indicates that the intrusive anomaly placed at this depth and dipping 6.5° north gives travel times close to the observed travel times. This picture is consistent with the regional structure as presented by Hill (1969), although the 7.0 km/sec layer would have to approach the surface within the rift zone.

Figure 10. Crustal sections from seismic refraction.

CRUSTAL SECTIONS FROM SEISMIC REFRACTIONS

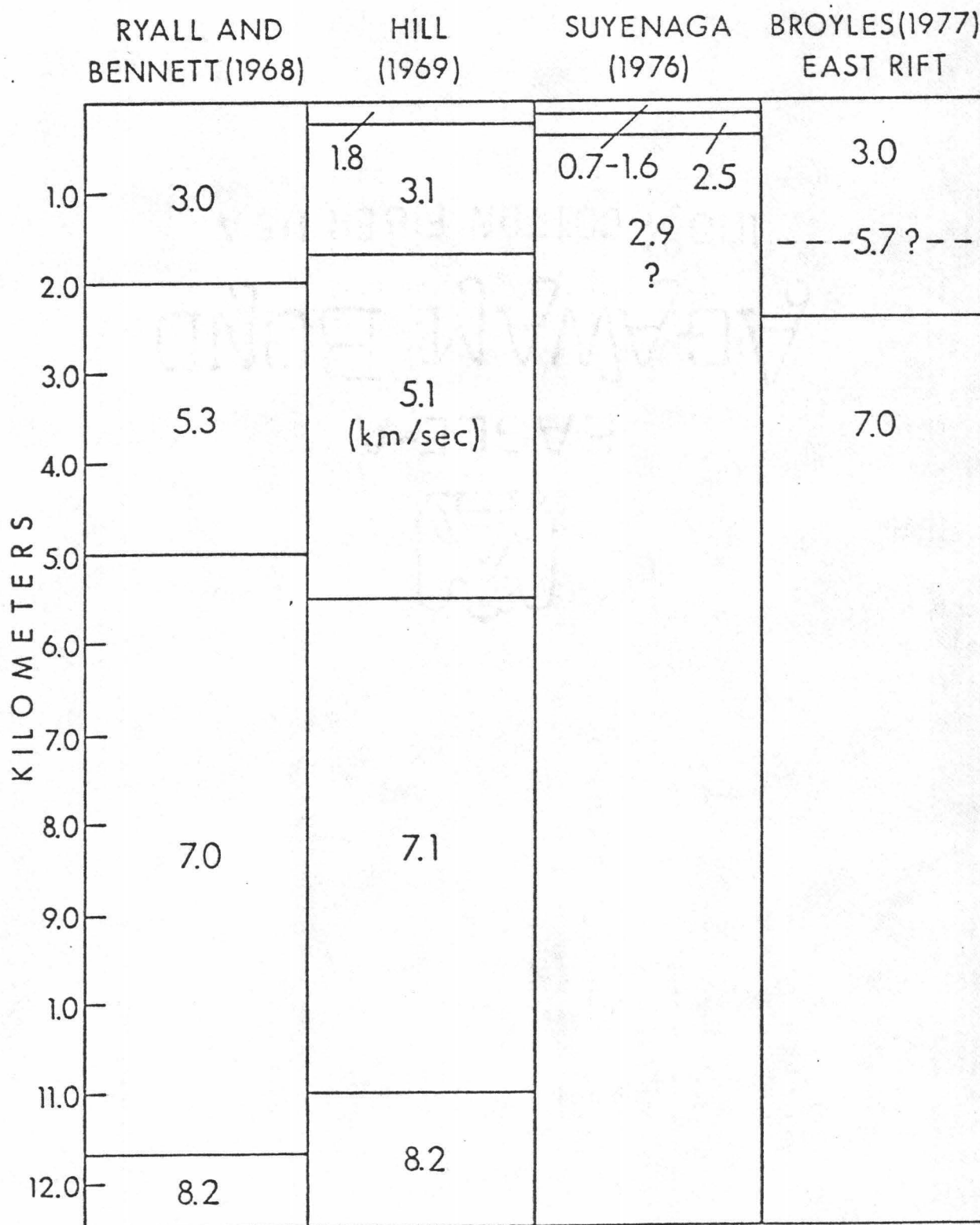


TABLE 1

Travel Times for the 1977 East Rift Refraction

Refraction Line	Shot Point	Travel Time (Seconds)
EW	2	$T = 1.40 + \Delta/6.76$
	3	$T = 1.40 + \Delta/6.98$
	4	$T = 2.00 + \Delta/8.23$
		$T = 1.70 + \Delta/6.83$
	5	$T = 2.20 + \Delta/8.23$
		$T = 2.00 + \Delta/7.27$
NS	1	$T = 0.00 + \Delta/3.00$
		$T = 1.00 + \Delta/5.25$
	2	$T = 0.15 + \Delta/3.00$
		$T = 1.10 + \Delta/5.64$
	3	$T = 0.45 + \Delta/3.43$
		$T = 1.35 + \Delta/5.71$
	4	$T = 1.45 + \Delta/5.70$
5	$T = 1.75 + \Delta/5.83$	
6	$T = 2.65 + \Delta/7.03$	
7	$T = 2.80 + \Delta/7.10$	

Gravity Data and Analysis

In June of 1975, a gravity survey of the Puna district was undertaken by four members of the Hawaii Institute of Geophysics (Furumoto, 1976). Over a hundred stations were occupied with an average grid spacing of 0.5 kilometers using La Coste Romberg and Worden gravity meters.

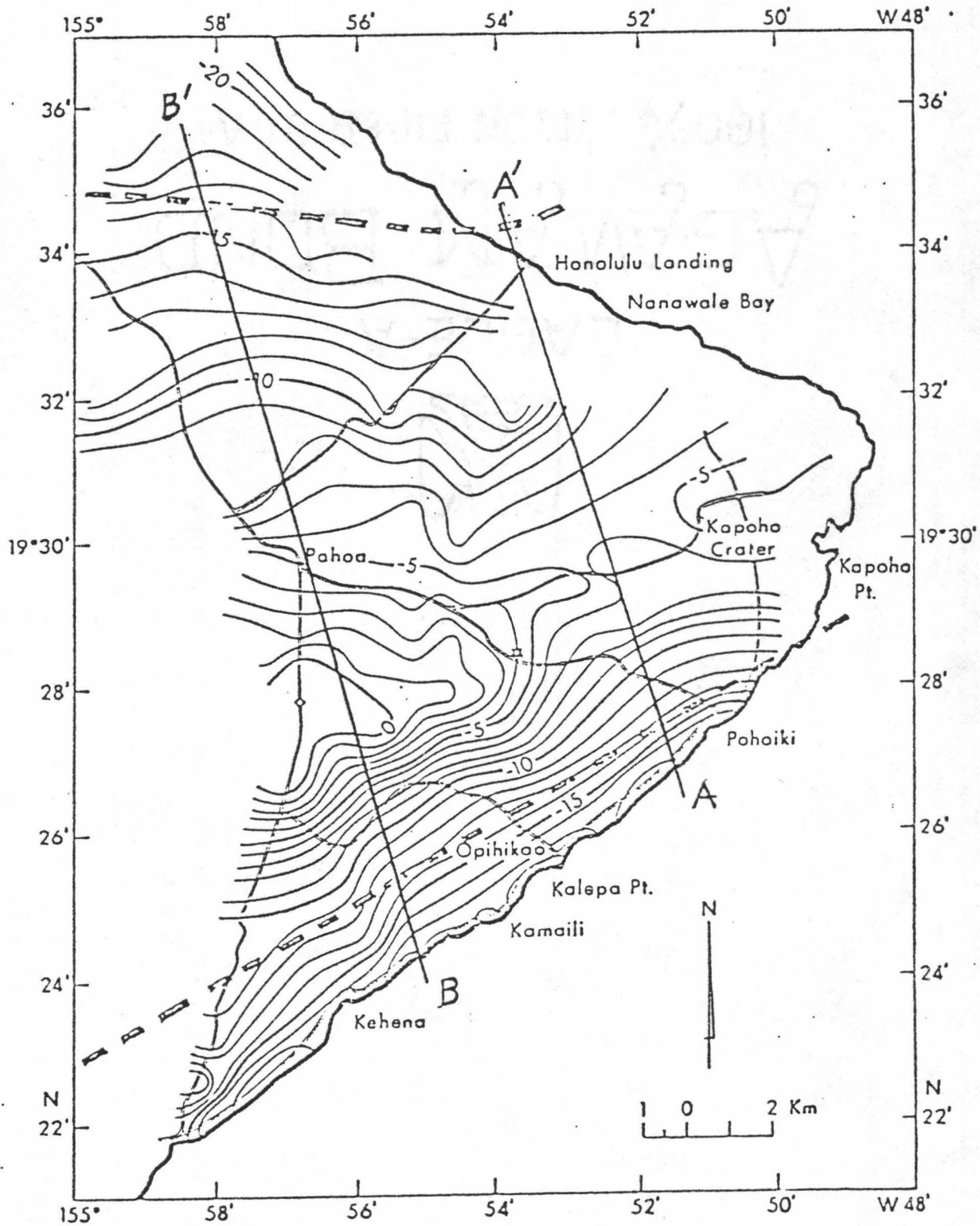
The elevations for the survey were taken from topographic maps of the region as there were bench and survey markers along the highway. The bench marks were used for the gravity stations as the elevations had to be precisely determined (Furumoto, 1976).

Terrain corrections were made using the technique of Kane (1962) out to a 30 kilometer radius (Furumoto, 1976). To correct for the mass of the ocean, terrain corrections were applied using Hammer's (1939) zone charts that included data from zone E to zone M taken from bathymetry charts (Furumoto, 1976).

A variety of Bouguer gravity maps were prepared for the Puna region (Furumoto, 1976). Figure 11 is a Bouguer map corrected for terrain and mass of the ocean using a surface density contrast of 2.3 g/cc. The estimated accuracy of this map is to ± 0.1 mgal (Furumoto, personal comm., 1977).

On this Bouguer map (Fig. 11), two profiles were constructed which are shown by the lines A'-A and B'-B. The surface trend of the anomaly shows a narrowing of the contours towards the southeastern extension of the rift. The narrowing of gravity contours is also

Figure 11. Bouguer gravity map of Puna with 1 milligal contours and corrected for the air-ocean interface (Furumoto, 1976). The dotted lines indicate the boundaries of the anomalous intrusive mass as inferred from seismic refraction and gravity interpretation.



revealed in Kinoshita's (1965) Bouguer gravity map of the island of Hawaii (Fig. 12). The data spacings here are 2 kilometers and a high of 275-280 mgals is revealed extending along the east rift.

A variety of models were devised in an attempt to match the observed Bouguer anomalies along the profiles B'-B and A'-A. First attempts at modeling used the approximate method as proposed by Skeels (1963) giving a rough idea of the subsurface structure of the anomalous body (Furumoto, 1976). The first attempts did not have the seismic data that now exists and refined studies using appropriate depth control could not be made.

With the new seismic data and more refined magnetic data (Norris, 1976) on hand, more extensive modeling of the intrusive body was attempted. After obtaining the various layer velocities and depths from the seismic work as discussed earlier, the gravity modeling was undertaken using two dimensional type computer programming (Talwani, 1958). This method used various polygons of different shapes placed at different depths and orientations.

As for appropriate depths, the top of the 7.0 km/sec layer was calculated from refraction data to be 2.5 km at the geothermal well site or 2.3 km below the sea level datum plane.

Models for profile B'-B as well as for A'-A used a depth of 2-3 km to the top of the anomaly with the lower limits of the intrusion placed at 4.0-6.0 km in the model depending upon the density contrast needed to match the observed Bouguer gravity field (Figs. 13 and 14).

Figure 12. Bouguer map of the island of Hawaii from Kinoshita (1965).

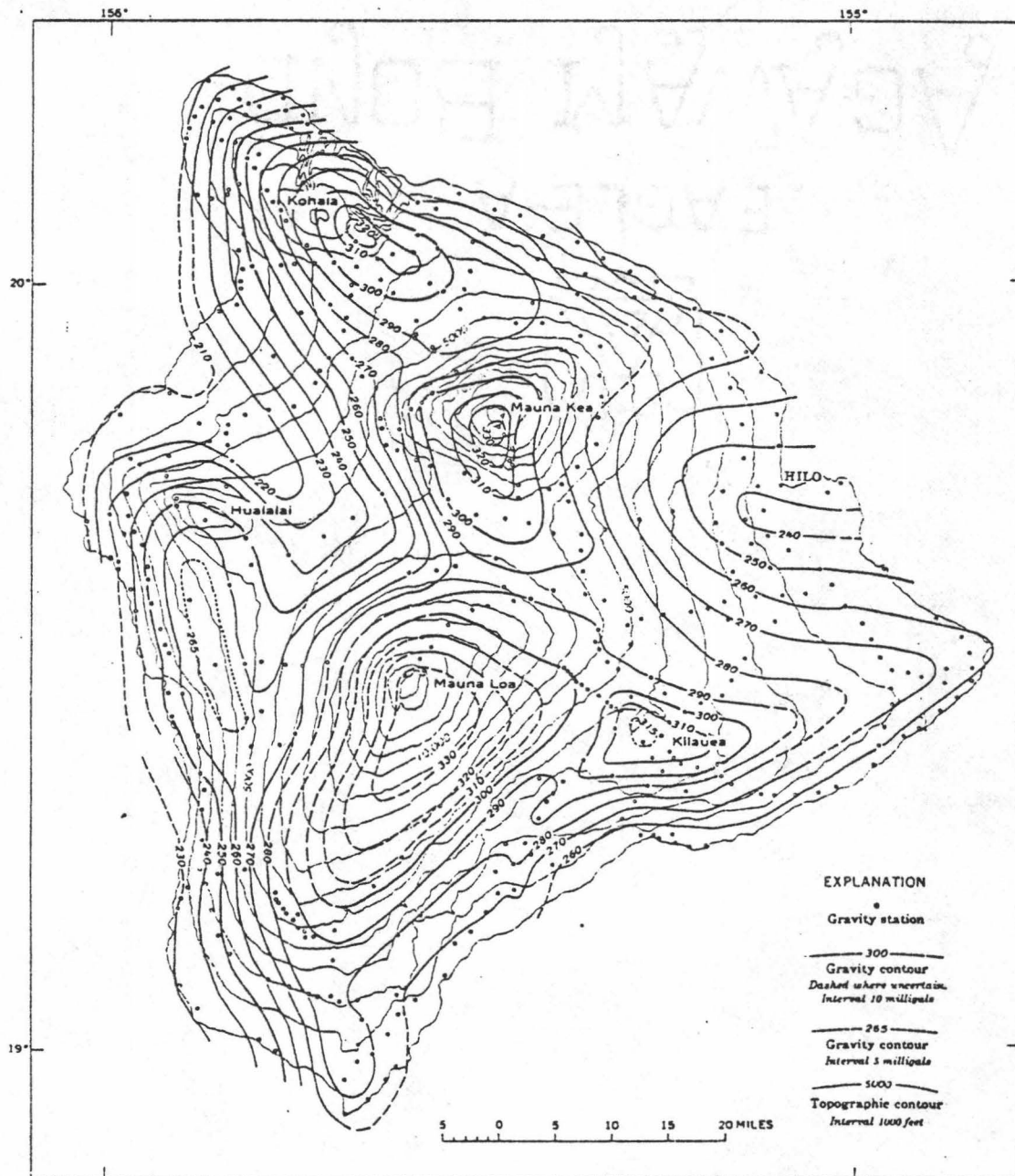


FIG. 1. Bouguer gravity-anomaly map of the island of Hawaii.

There was little seismic control on the width of the anomaly other than a break from low to high velocity material appeared to occur between stations T3 and M on the NS line, profile B'-B (Fig. 12). On the map of Puna, this break appears to occur 2-4 km from the coast on the NS line (Figs. 2 and 13). On the models, however, a good approximation to the observed field was obtained by placing the southern limit of the anomaly at slightly less than 2 km from the coastline.

The next procedure in the gravity modeling was to select an appropriate density contrast for each model. A uniform density contrast was selected for all models as information is not yet available on lateral variations of density even though there are probably density variations within the rift (Macdonald, personal communication, 1977).

Density contrasts of 0.30-0.90 were initially selected for the models but narrowed to the range of 0.40-0.60 in later analysis as the latter values were more in line with our seismic data as well as previous studies, Rose, Woollard and Strange (1965) in their analysis of the volcanic intrusions of the Hawaiian Islands and Furumoto (1976) in the analysis of gravity from the Puna region.

To arrive at density contrasts compatible with our seismic data, the technique used was as follows. If the velocity of the second layer was 5.7 km/sec then the density would correspond to 2.7 g/cc from studies of Hawaiian basalts by Manghnani and Woollard (1968). The velocity of the intrusive layer was 7.0 km/sec giving a density

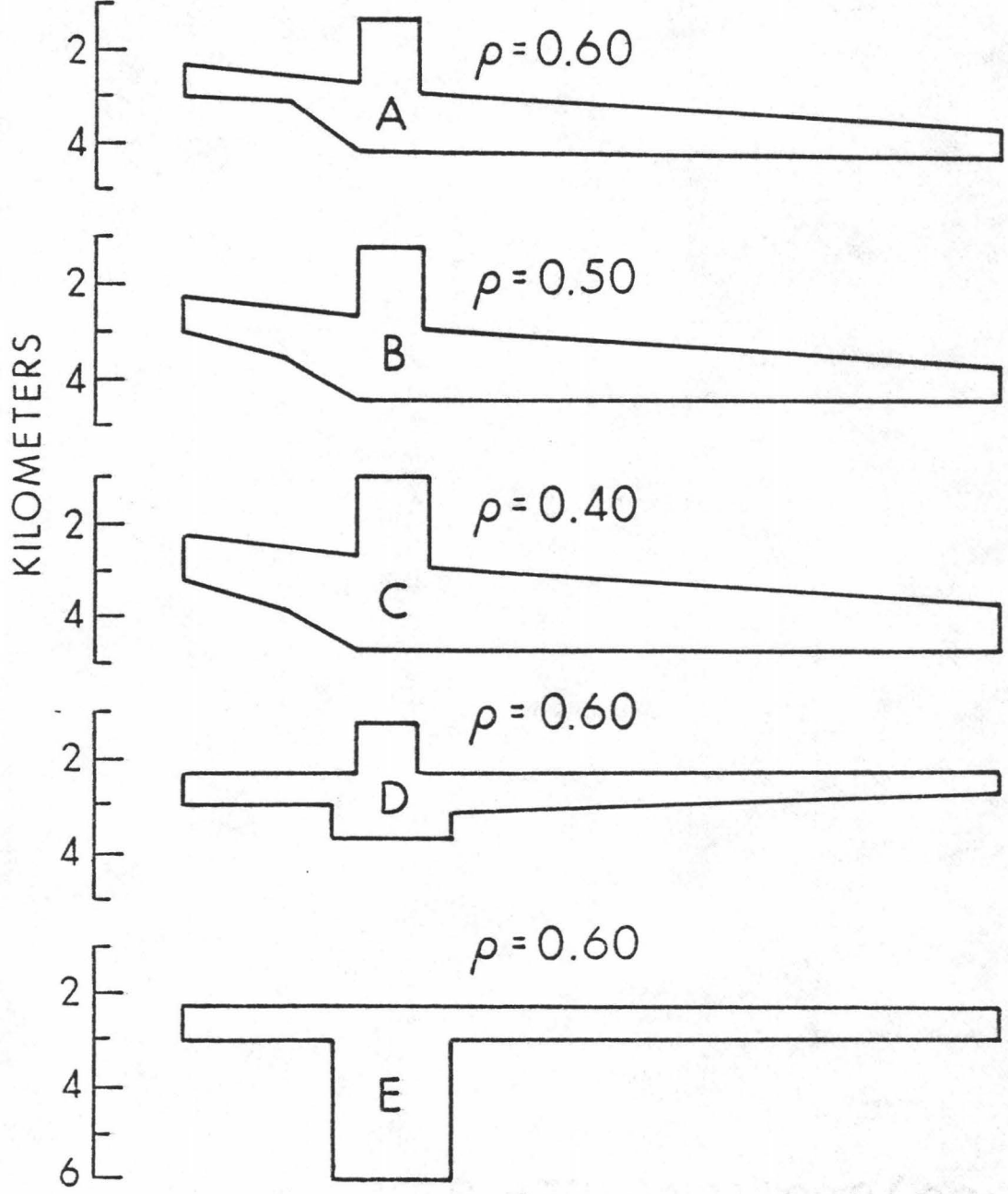
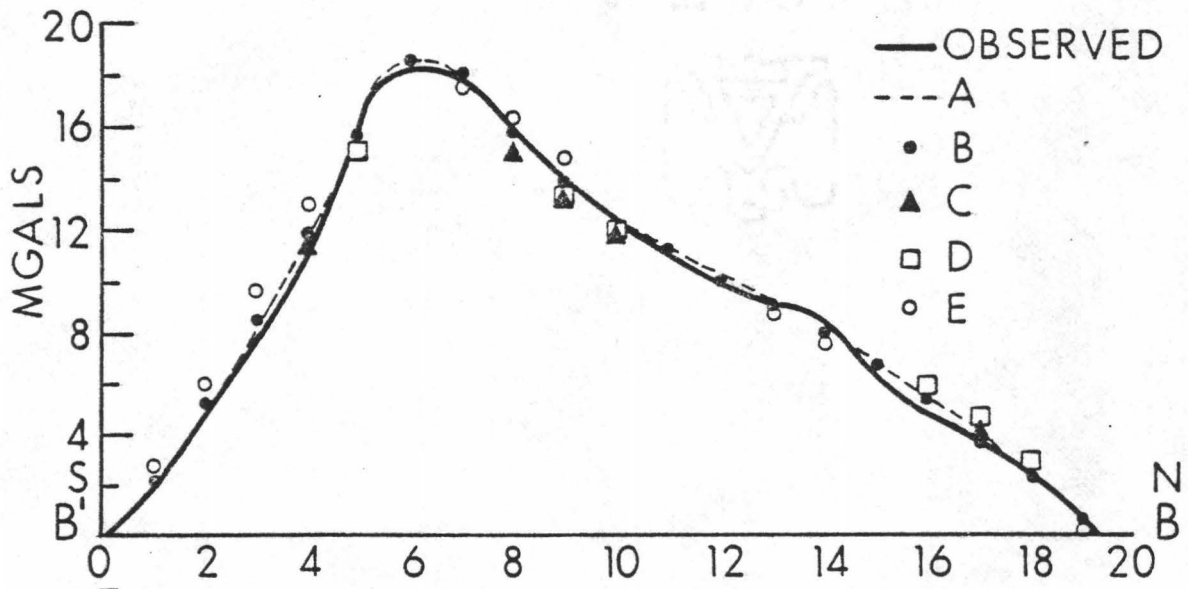
of 3.1 km/sec extending the table by Manghnani and Woollard (1968). The difference in these two densities or density contrast is then 0.40. If, however, the true velocity of the second layer was 5.1 km/sec as Hill (1969) indicates, then our appropriate density contrast would be 0.60 as 5.1 km/sec gives a density of 2.5 g/cc (Manghnani and Woollard, 1968).

Models for the line B'-B used a uniform density contrast and a depth of 2-3 km to the top of the anomaly. The lower limits of the intrusion were placed at 4.4-5.0 km to match the observed gravity field.

In models A, B and C the top of the main body of the anomaly, excluding the chimney slopes 6-7 degrees towards the north. A chimney was placed on models A-C that approach the surface to a depth of just over 1 km. This chimney is believed to be a local feature, a shallow dike complex responsible for a high magnetic intensity in the Leilani region, Figure 16 (Norris, 1976). The chimney effect is not delineated by seismic refraction but is inferred from magnetic data (Norris, 1976) and by superimposing this "plug" on the main intrusive body, the observed gravity field may be closely matched if the bottom of the model anomaly is allowed to go no deeper than 5.0 km, the proposed average depth of the ancient ocean floor (Macdonald, 1965).

Models B and C (Fig. 13) assume the same constraints as model A, except for uniform density contrasts of 0.50 and 0.40, respectively.

Figure 13. Gravity models for the profile B'-B, Figure 11.



Notice that the lower the density contrast becomes, the deeper and more massive the model intrusive anomaly becomes.

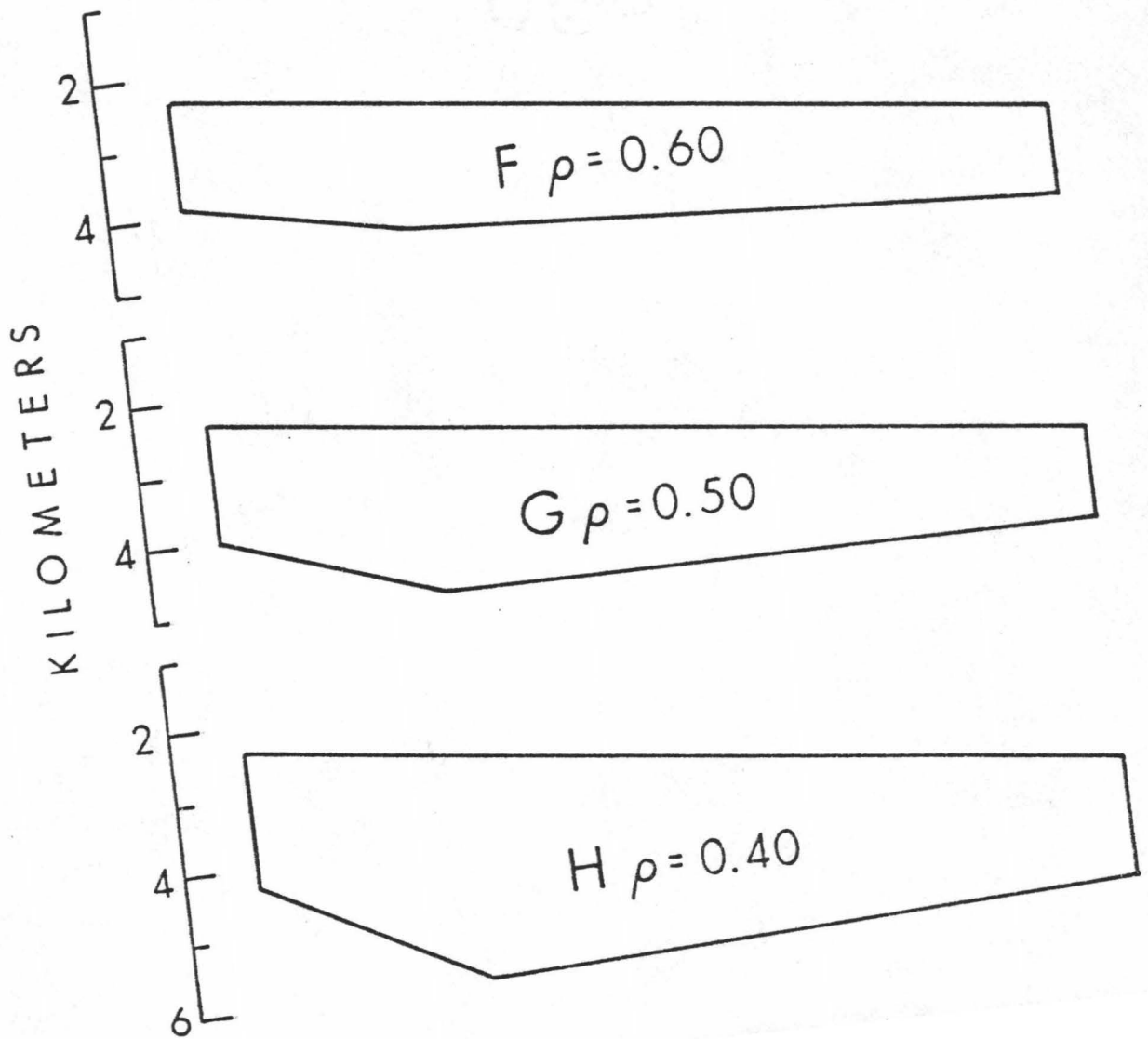
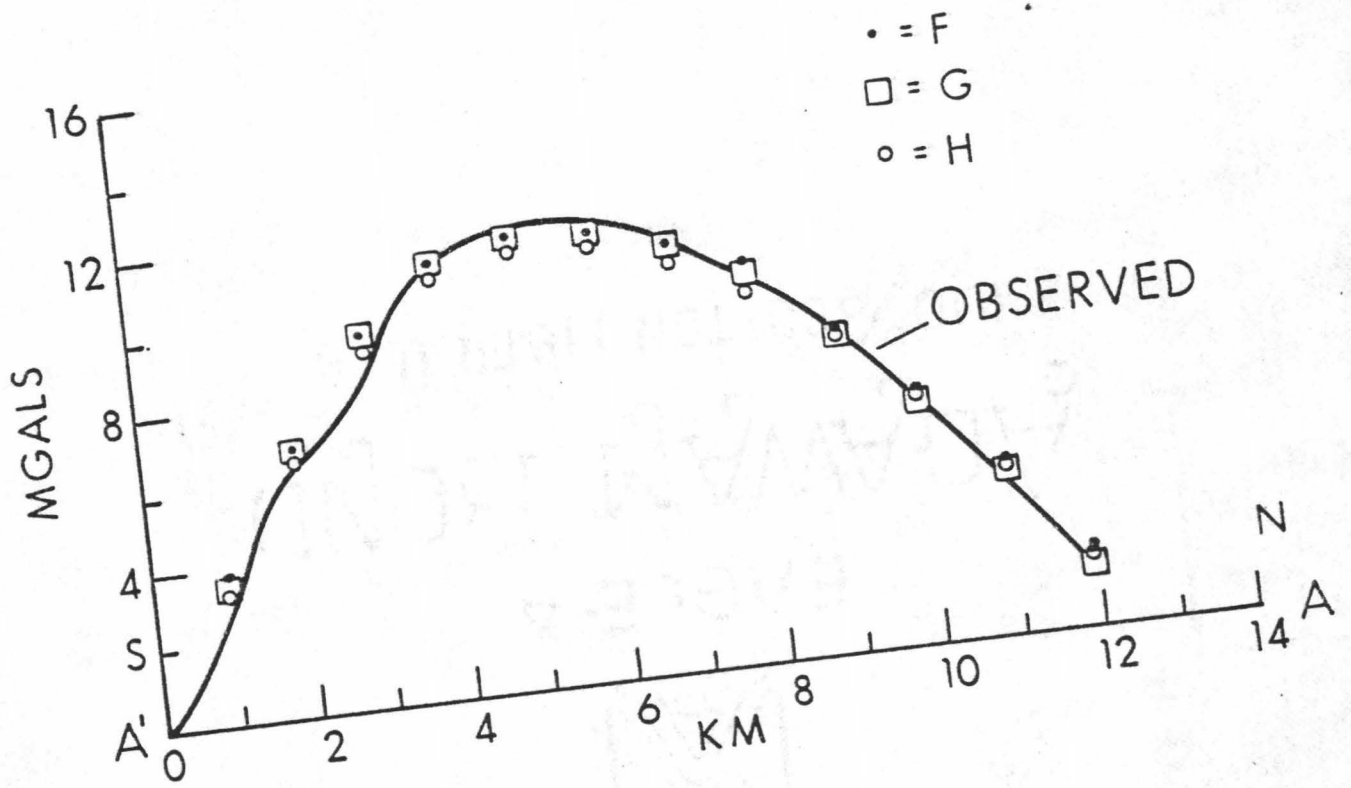
Model D assumes a uniform depth of 2.3 km to the top of the main body with a chimney approaching the surface to about 1 km with a region of excess mass below; again the anomaly fits the observed gravity well. This model was constructed to show the distribution of mass necessary, if all the observed velocities are assumed to be real values with no velocity contrasts due to anomalous dips.

Model E also assumes a uniform depth of 2.3 km to the top of the anomaly. If the chimney is not placed atop the main intrusive body, then an excess of mass is necessary below the greatest amplitude of the observed gravity field.

Profile A'-A gravity was also closely matched with models F, G and H (Fig. 14) of density contrasts varying from 0.40-0.60 using the same depth controls as for models along profile B'-B. Three models are shown which assume a 6-7 degree dip as discussed earlier. A variety of models fit this picture as well but with the seismic depth controls, the following are differences in this line as compared to B'-B.

- (1) For the same depth of anomaly, the width of the intrusive zone is narrower, 12 km as opposed to 17 km.
- (2) A mass of more uniform shape is needed for A'-A.
- (3) A chimney is not necessary to produce the highest part of the observed gravity anomaly; there is not the magnetic evidence for this feature that there was on line B'-B.

Figure 14. Gravity models for profile A'-A, Figure 11.



The lowest part of the intrusion extends to depths of 4-5 km as for line B'-B.

All of the models shown in both figures assume a second layer of velocity 5.1-5.7 km/sec. It is highly unlikely that the 7.0 km/sec layer has no second layer between it and the surface material of velocity 3.0 km/sec as this would not be in agreement with prior surveys (Ryall and Bennett, 1968; Hill, 1969) and would necessitate density contrasts as high as 0.80-0.90.

Models were also attempted for narrow and steeply dipping intrusive bodies. In general, although it is possible to match the greatest observed gravity values, the calculated field falls off much more rapidly than the observed field with distance from the center of the maximum observed values.

DISCUSSION

COMPARISON WITH MAGNETIC ANALYSIS

Magnetic surveys over the east rift zone have been conducted by Malahoff and McCoy (1967) and Norris (1976). The survey by Malahoff and McCoy (1967) included a land survey recorded by an airborne magnetometer 2700 m above the topography and compared with the total force magnetic readings (Fig. 15). The seaward magnetic anomalies were recorded at sea level and were corrected for the daily variation of the total force of the earth's magnetic field (Malahoff and McCoy, 1967). The steepest gradients occur some 6 km off the coastline of Cape Kumukahi; inland, the gradients become smaller and the total magnetic intensity less.

The magnetic survey by Norris (1976) was in the Puna region. Highs are observed both in the western section of Puna and at Kapoho crater (Fig. 16). A corresponding low is observed in the western sector and although there are no corresponding lows observed for Kapoho crater, we believe (Furumoto and Broyles, 1977) that a low trend is evident in the offshore data of Malahoff and McCoy (1967) just NE of Cape Kumukahi. There is a low density of ground measurements south of Kapoho crater (Fig. 15), however.

Modeling techniques as described by Vacquier et al. (1951) were used for the Puna region by Norris (1976) and symmetry of the magnetic field surrounding the dipole suggests that the depth here is $1/2$ the width of the anomaly. Although the boundaries here are

Figure 15. Seaborne magnetic anomalies observed over the Puna submarine ridge (total force in gammas). Land anomalies were recorded by an airborne magnetometer 2700 meters above topography from Malahoff and McCoy (1967).

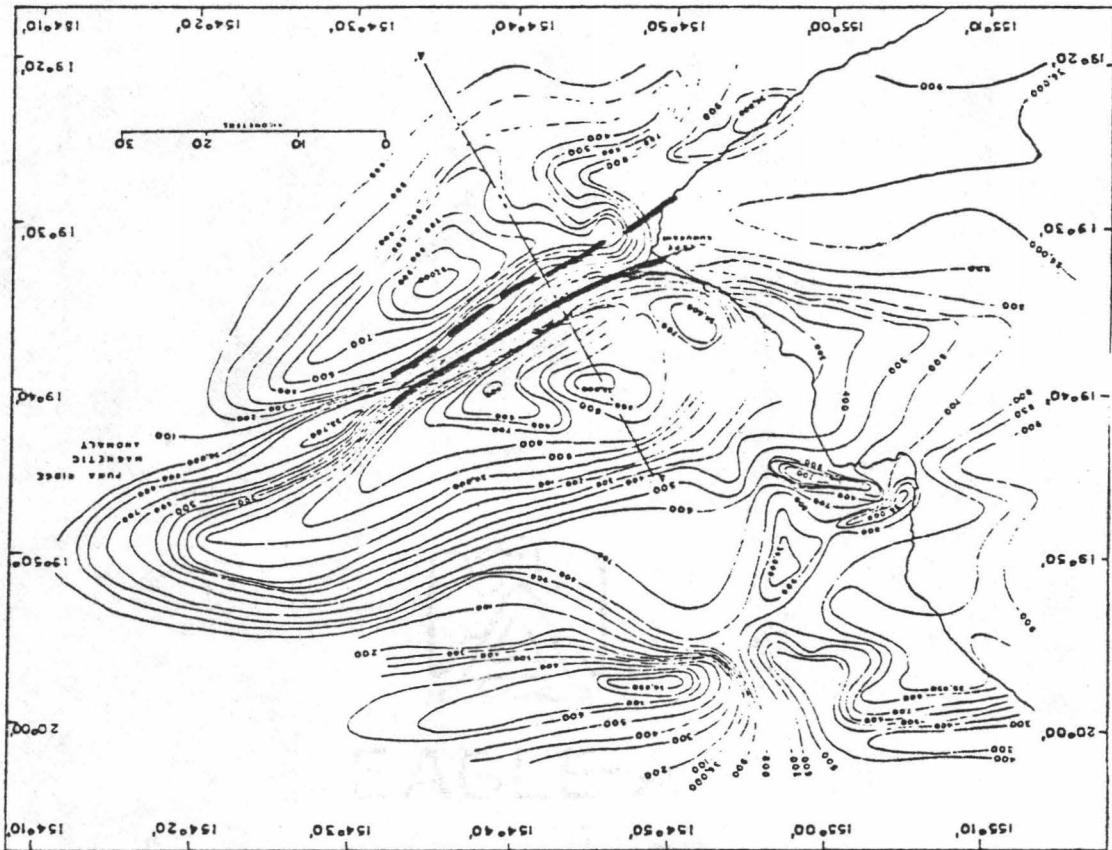
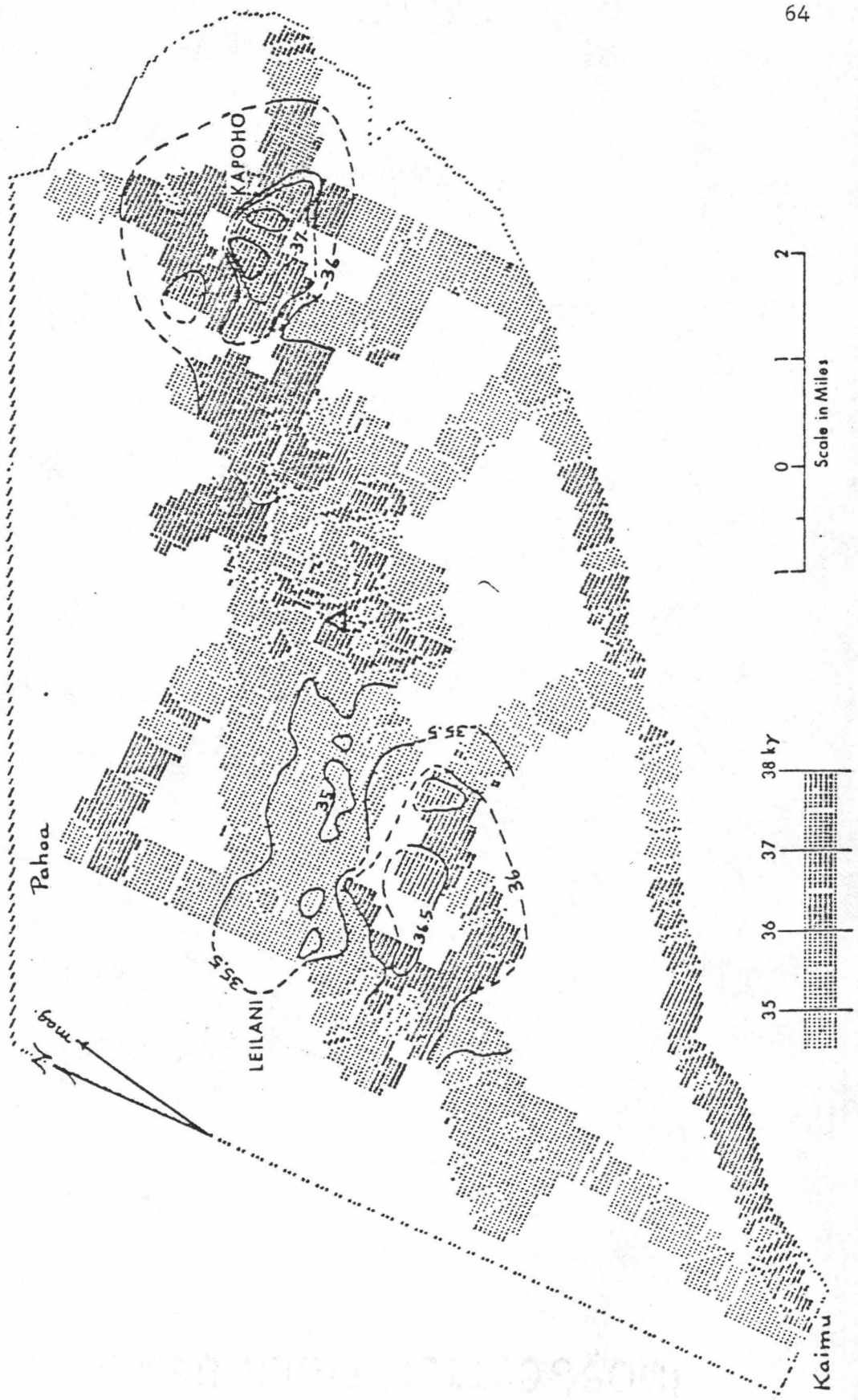


Figure 16. Total magnetic intensity at ground level with 500 gamma intervals. Inked contours reveal Leilani and Kapoho anomalies (from Norris, 1976).



rather diffuse, a width of 1 1/2-2 km would place the anomaly 500-700 meters deep using an inclination of 30 degrees for the earth's magnetic field in the region (Norris, 1976).

As a comparison here, gravity models as discussed in the previous section give a better fit to the observed data if the depth to the anomaly is placed at 1.0-1.3 km, however.

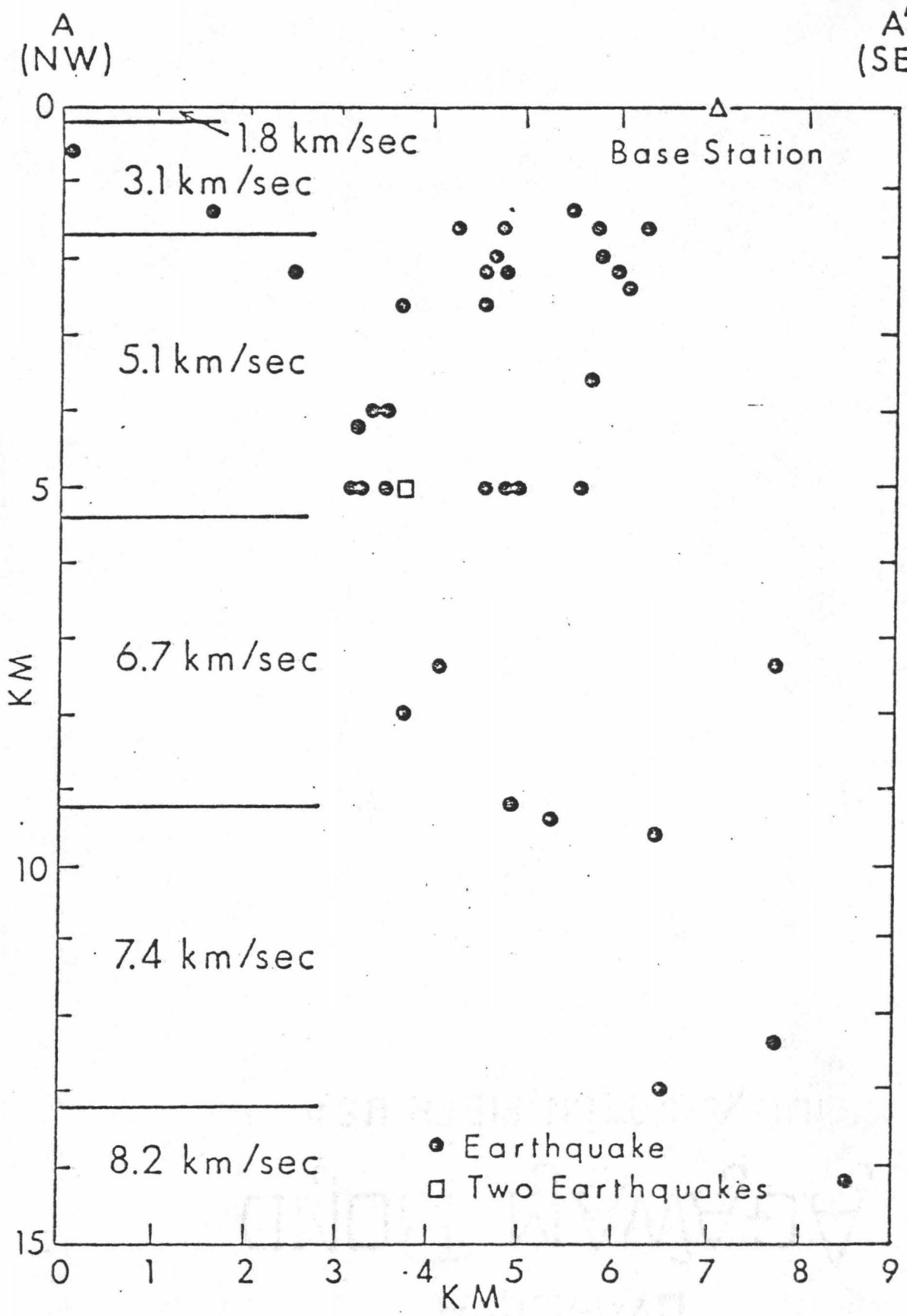
COMPARISON WITH PASSIVE SEISMIC SURVEYS

A microearthquake survey was conducted from August 16 to September 9, 1974 in Puna by Suyenaga (1975) using a seven seismometer array, Figure 17. The hypocenters were originally calculated by a computer program with a crustal model using a layer of 6.8 km/sec at 4 km (Hill, 1969). A more up to date analysis of the earthquake distribution is now underway based on the new refraction profiles (Suyenaga, personal communication, 1977. The results of the distribution of microearthquakes in the array area as given by Suyenaga (1975) are (Fig. 17):

- (1) the hypocenter positions on a plane perpendicular to and directly beneath the rift zone span approximately 3 km. Below 7 km depth, the hypocenters are scattered vertically beneath the rift and slightly to the south and may outline the lower extent of the intrusions.
- (2) there is a clustering of activity outlining the extent of the geothermal reservoir.
- (3) there is evidence of deeper activity on a plane dipping from NW to SE that may be tectonically controlled.
- (4) the majority of the microearthquakes lie within the intrusive zone outlined by gravity data at a depth of 1-3 km.

A survey of the ground noise levels in the Puna region was conducted by Norris (1976). The results indicated high ground noise in the vicinity of the geothermal reservoir with a persistent band at 4 Hz. A possible conclusion was the high ambient noise is related

Figure 17. Depth of foci of microearthquakes from Suyenaga (1976). The crustal model was inferred from Hill (1969) by Suyenaga (1976).



to geothermal processes within the well reservoir, however, this study emphasized that the noise may be amplified in the region of the reservoir due to the nature of the fractured rocks (Norris, 1976). Thus the amplified noise may not be more significant than background noise levels.

COMPARISON WITH PETROLOGY

Various studies have been made of the rocks, cores and cutting chips that have been taken from the Hawaii Geothermal Project drill hole (Fig. 2, pt. A). Petrological analysis of the core samples was made by Stone (1977) and velocity measurements of the core samples by Rai (1977).

From refraction studies it is known that the upper surface structure of the east rift is of low velocity, ranging from 0.7-1.6 km/sec (Suyenaga, 1976). An analysis of rocks in the upper 875 m of the well indicates that vesicularity or pore space varies from moderate to high or about 30% (Stone, 1977). These studies show that the lava flows near the surface are highly fractured and permeable. The lava flows as evidenced from the cores and cutting chips from the geothermal well are unaltered down to 675 m and consist of quartz-normative tholeiitic basalts (Stone, 1977).

Below the surface layers, velocities of 2.5 km/sec and 2.9 km/sec are observed on the flank and 3.1 km/sec on the rift (Suyenaga, 1976). These higher velocities do not reflect a major change of lithology, other than alteration (Stone, 1977) but are probably associated with saturation at the water table (Rai, personal communication, 1977). In other studies, basalt velocities increased from 4.1 km/sec when dry to 6.0 km/sec when saturated from samples off the East Pacific Rise (Christensen and Salisbury, 1975).

Figure 18 correlates the seismic velocity structure from the field and the velocity structure from the core specimens as measured in the laboratory. Although there are no definite breaks in the seismic velocity that correlate with changes in lithology, there are broad changes in the rock structure that may be reflected in the observed seismic velocities.

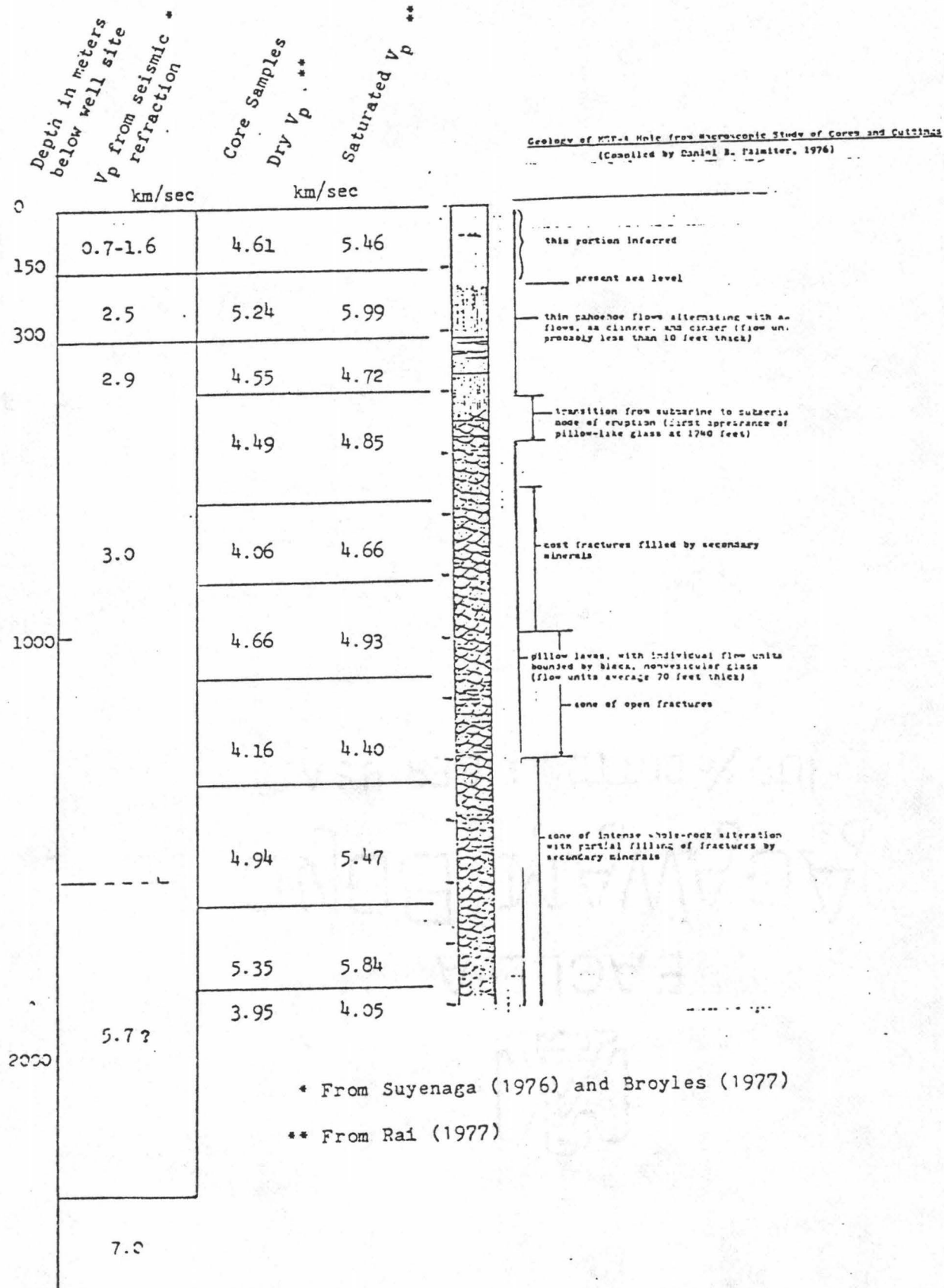
- (1) At 318 m in the well hole, the first signs of alteration are found. In this section, olivine phenocrysts are completely altered to montmorillonite (Stone, 1977).
- (2) At about 1400 m, a zone of intense whole rock alteration begins with partial filling of fractures by secondary minerals and the alteration is found to increase consistently with depth (Stone, 1977).
- (3) At 1960 m into the well, low grade metamorphism occurs where highly altered rocks of type amphibole, zeolite, gibbsite and siderite are located (Stone, 1977). Notice that the depth to the 7.0 km/sec material as revealed by refraction data lies below the deepest core sample.

After examination of Figure 17, one can observe that there are major differences in the velocity structure as determined from refraction data (Suyenaga, 1976; Furumoto and Broyles, 1977) as compared to the laboratory data from Rai (1977). The field data measures the bulk velocity of the rocks whereas the laboratory measures the particle velocity. We would expect to see such large variations because the rocks are fractured and broken up near the

Figure 18. Petrology and velocity structure of the east rift.

This is a crustal section of the HGP-A well hole correlating the geology of the well hole with the velocities from seismic refraction and laboratory measurements.

CRUSTAL SECTION OF HGP-A HOLE



surface and will not transmit sound waves as effectively as the smaller crystals and rock fragments that are still intact. One should keep in mind that the compressional velocity varies considerably as the pressure closes up the fractures (Manghnani, 1968).

CONCLUSIONS REGARDING THE STRUCTURE
OF THE EAST RIFT

In summary the following are conclusions regarding the structure of the anomalous area of the east rift as delineated by the various geophysical methods as described in this thesis:

- (1) The zone of dense material is located at depths of 2-3 km reaching depths of only 1 km in some regions (Fig. 19). The bottom of the complex is probably at 4-5 km.
- (2) The lateral extent of the rift zone in the Puna region is much wider 12-17 km than the surface expression of the rift. A large amount of the intrusive mass appears to be concentrated towards the south side of the rift in a zone 1-3 km wide (Fig. 13). This zone may be a region of active dike intrusion.
- (3) Assuming a second layer velocity of 5.1 km/sec and the intrusive layer velocity of 7.0 km/sec, the density contrast between both layers would be 0.60.
- (4) The upper surface of the main dense zone appears to have a gentle 6-7 degree northward slope. This northward slope could produce the anomalous velocity of 5.7 km/sec as observed only on the NS line. This northward sloping structure may be modeled to fit the observed Bouguer gravity field (Fig. 13). This interpretation agrees with that of Swanson et al. (1976). These authors postulate

that a wedge-shaped intrusive dike mass with a shallow north face and a steep south face would explain the asymmetric observed gravity field. The observed gravity field has steeper gradients south of the rift zone (Fig. 11). Swanson et al. (1976) believe that such a wedge shaped structure would be the product of southward and upward migration of progressively younger dikes. In this model there would be lateral growth of the rift to the south as gravity would favor south-southeastward displacement. Younger dikes would be preferentially formed southward as the lava flows for these dikes that intrude at progressively shallower depths cover up the older flows. An alternate explanation for the northward sloping structure, if in fact real, has been proposed by Macdonald (personal communication, 1977). In this scheme, the development of Kilauea volcano, a topographic high, on the slopes on the older Mauna Loa cone would produce such a structure.

- (5) The gravity high (Figs. 12 and 13) follows boundaries close to those of the magnetic and topographic highs.
- (6) The edge of the dike complex occurs on the boundaries of magnetic lows as a probable result of strong susceptibility contrasts between the intrusive and surrounding basalts. The magnetic high of the Puna ridge that may have a composite plug and dike complex located within it (Malahoff and McCoy, 1967) merges with the intrusive dikes of the Puna rift zone.

- (7) The region of high seismic velocity appears to be located within the zones of high gravity and magnetization contrasts.

There is strong evidence for a shallow magma reservoir beneath the summit of Kilauea volcano. From our seismic and magnetic data we believe that the depth to the main intrusive dike complex is about 2 km and probably reaches depths of 4-5 km. The bottom of the complex would agree with the ideas of the growth of Hawaiian volcanoes that form by extruding onto the ancient ocean floor, the average depth being 5 km (Macdonald, 1965).

There is also geophysical evidence for a group of vertical plugs or dikes whose tops come to within 1 km of the surface in some regions such as Leilani Estates. This depth agrees with prior studies of finite element modeling as described by Dieterich and Decker (1975) and magnetic analysis by Norris (1976).

Such high velocity material close to the surface in volcanic or rift regions has been detected in other refraction studies as well. In the analysis of the structure of the Koolau volcano from seismic refraction studies, there are indications of material with velocities as high as 7.7 km/sec reaching depths less than 2 km (Furumoto et al., 1965).

Rift activity usually occurs contemporaneously with abrupt subsidence of the summit region (Eaton, 1962; Wright, Kinoshita and Peck, 1968). At these periods, magma is believed to intrude laterally into the rift and is thought to take the form of thin, steeply

dipping, blade-like dikes. The dike propagation is believed to be dominantly horizontal (Fiske and Jackson, 1972); however, some dikes probably start their formation at high levels and are fed directly from rupture of the reservoir complex. The regions of these dike intrusions correspond to lineations in the magnetic data (Furumoto and Broyles, 1977). The rift evidently narrows somewhat towards the sea as magma moves outward from the summit reservoir in conduits progressively losing volume to driving surface eruptions of gases and lava along the rift (Figs. 13 and 14).

A possible reason for more mass on the south side might be ponding of lava as a result of downslope movement. In fact, Moore and Krivoy (1964) in noting the parallelism of the Hilina fault zone, suggest that the rift zone has originated due to "seaward sliding under the influence of gravity", a mechanism that could cause the propagation of lava downslope. Gravity modeling has indicated that a greater distribution of mass is necessary closer to the south end of the profiles B'-B and A'-A (Figs. 13 and 14). Another explanation for the excess of mass towards the south side of the rift is that the loss of gases as the lava moves downslope would cause the lava to become more compact and denser (Macdonald, personal communication, 1977).

There is evidence that the rift structure is regionally as well as locally affected by faulting. Ryall and Bennett (1968) interpreted the offset in the Hilo-Kalae travel-time data as displacement along a fault dipping east or northeast from Kilauea and related to

the northeast rift zone of Mauna Loa or the east rift zone of Kilauea. Our data suggests faulting for NS lines shot 4 and shot 5 (Fig. 8). This shooting is unreversed and the actual throw of the suspected fault cannot be determined.

Faulting associated with the Kalapana earthquake of 1975 occurred to the south of the rift along the Hilina fault system (Tilling, 1976). The new surface breakage took place within a series of steeply dipping normal faults along preexisting fault traces with displacements to the south.

The depth of the anomaly that has been calculated with seismic and gravity constraints is also consistent with an estimation of the Curie point depth. Based on a study of the well temperature profile (Furumoto and Broyles, 1977) and assuming the heat flux at the bottom of the well to be 30 h.f.u. (heat flow units), one would arrive at a temperature of 540°C at a depth of 2470 m below the well. This study also assumes the appropriate value of thermal diffusivity of rocks (Rai, 1977) and a temperature gradient of $470^{\circ}\text{C}/\text{km}$ at the bottom of the well hole (Furumoto and Broyles, 1977). A temperature of 540°C is believed to be the Curie point for rocks in this region (Zablocki and Tilling, 1977).

The results of the present studies are summarized in a model (Fig. 19) that shows the structure of the dike complex beneath the east rift zone. The following features are indicated on the model:

- (1) The main intrusive complex is located on the slopes of Mauna Loa with a thickening of the complex southeastward.

- (2) A shallow dike complex rests atop the main intrusive complex at a depth of 1 km and is responsible for the magnetic highs and lows over the western section of Puna.
- (3) The geothermal reservoir is a region of fractured and more or less permeable rocks within the dike complex.
- (4) The ancient seafloor forms the lower limit of the dike intrusions.
- (5) The surface of the dike structure dips to the north at a shallow angle and abruptly to the south.

Figure 19. Structure of the east rift from Furumoto and
Broyles (1977).

SOUTH

NORTH

GEOHERMAL RESERVOIR

SHALLOW DIKE COMPLEX

1955 FLOW

LAND TOPOGRAPHY

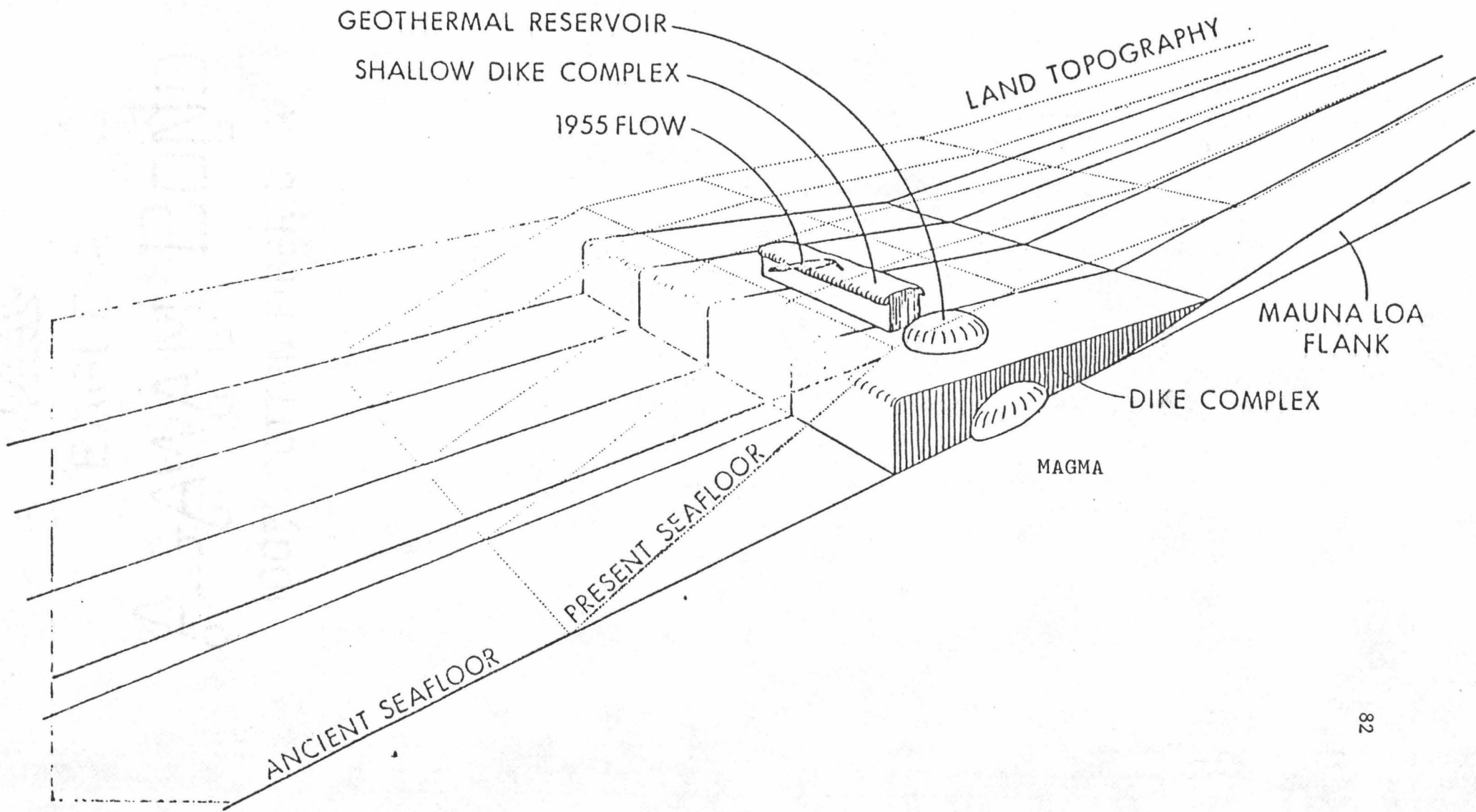
MAUNA LOA
FLANK

DIKE COMPLEX

MAGMA

PRESENT SEAFLOOR

ANCIENT SEAFLOOR



REFERENCES

- Christensen, N. I. and M. H. Salisbury, Structure and constitution of the lower oceanic crust; *Rev. Geophys. and Space Phys.*, v. 13, 57-86, 1975.
- Dieterich, J. H. and R. W. Decker, Finite element modeling of surface deformation associated with volcanism; *Jour. Geophys. Res.*, v. 80, 4094-4102, 1975.
- Dobrin, M. B., *Introduction to Geophysical Prospecting*; McGraw Hill Book Co., New York, 446 p., 1960.
- Eaton, J. P., Crustal structure and volcanism in Hawaii, in *The crust of the Pacific basin*, Am. Geophys. Union Mono. 6, Washington, D. C., 1962.
- Fiske, R. S. and E. D. Jackson, Orientation and growth of Hawaiian volcanic rifts; the effect of regional structure and gravitational stresses; *Proc. Roy. Soc. Lond.*, 299-326, 1972.
- Fiske, R. S. and W. T. Kinoshita, Inflation of Kilauea volcano prior to its 1967-1968 eruption; *Science*, 165, 341-349, 1969.
- Furumoto, A. S. and M. L. Broyles, Dimensions and thermal processes of the magma conduits underlying the east rift zone of Kilauea volcano, *Inter. Assoc. of Seis. Ear. Int., Volcan. and Chem. Ear. Int., Joint General Assemblies*, Durham, England, 1977.
- Furumoto, A. S., R. Norris, M. Kam and C. Fenander, Progress report, Gravity profile and the Intrusive zone, in *The Hawaii geothermal project, Initial phase II progress report*, February 1976.
- Furumoto, A. S., N. J. Thompson and G. P. Woollard, The structure of the Koolau volcano from seismic refraction studies; *Pac. Sci.*, v. XIX, p. 306-314, 1965.
- Hammer, Sigmund, Terrain corrections for gravimeter stations; *Geophysics*, v. 4, p. 184-194, 1939.
- Hill, D. P., Crustal structure of the Island of Hawaii from seismic-refraction measurements; *Bull. Seis. Soc. Am.*, v. 59, p. 101-130, 1969.
- Kane, M. F., A comprehensive system of terrain corrections using a digital computer; *Geophysics*, v. 27, p. 455-462, 1962.

- Kinoshita, W. T., A gravity survey of the island of Hawaii; *Pac. Sci.*, v. 19, p. 339-340, 1965.
- Macdonald, G. A., The structure of Hawaiian volcanoes, Koninklijk Ndeerlandsch Geologisch Mijnbouwkundig Genootschap, *Verhandelingen*, v. 16, 274-295, 1956.
- Macdonald, G. A., Hawaiian calderas; *Pac. Sci.*, v. 19, p. 320-334, 1965.
- Malahoff, A. and F. McCoy, The geologic structure of the Puna submarine ridge, Hawaii; *Jour. Geophys. Res.*, v. 72, p. 541-548, 1967.
- Manghnani, M. H. and G. P. Woollard, Elastic wave velocities in Hawaiian rocks at pressures to ten kilobars, in the crust and upper mantle of the Pacific area; *Am. Geophys. Union Mono.* 12, v. 12, p. 501-522, 1968.
- Matthews, F. I. C., Tables of the velocity of sound in pure water and sea water for use in echo-sounding and sound ranging, publ. by the Hydrographic Depart. Admiralty, 1939.
- Moore, J. G. and H. L. Krivoy, The 1962 flank eruption of Kilauea and structure of the east rift zone; *Jour. Geophys. Res.*, v. 69, 2033-3245, 1964.
- Moore, J. G. and D. H. Richter, The 1961 flank eruption of Kilauea volcano, Hawaii; *Trans. Am. Geophys. Union*, v. 43, p. 446, 1962.
- Nettleton, L. L., *Geophysical prospecting for oil*; McGraw-Hill Book Co., New York, 444 p., 1940.
- Norris, R., Puna Magnetics; Progress report in, The Hawaii geothermal project, Initial phase II progress report, University of Hawaii, 148 p., 1976.
- Rai, C. S., Electrical and elastic properties of basalt and ultramafic rocks as a function of saturation, pressure and temperature, Ph.D. dissertation, University of Hawaii, 1977.
- Ryall, A. and D. L. Bennett, Crustal structure of southern Hawaii related to volcanic processes in the upper mantle; *Jour. Geophys. Res.*, v. 73, p. 4561-4582, 1968.
- Skeels, D. C., An approximate solution of the problem of maximum depth in gravity interpretation; *Geophysics*, v. 28, p. 724-735, 1963.

- Stone, C., Chemistry, petrography and hydrothermal alteration of basalts from Hawaii geothermal project well-A, Kilauea, Hawaii; M. S. thesis, University of Hawaii, 1977.
- Strange, W. E., G. P. Woollard and J. C. Rose, An analysis of the gravity field over the Hawaiian Islands in terms of crustal structure; *Pac. Sci.*, v. XIX, p. 381-389, 1965.
- Swanson, D. A., W. A. Duffield and R. S. Fiske, Displacement of the south flank of Kilauea volcano; The result of forceful intrusion of magma into the rift zones; Geological Survey Professional Paper 963, 1976.
- Suyenaga, W., The shallow seismic structure of the east-rift zone of Kilauea, Hawaii, unpublished report, 1976.
- Suyenaga, W. and A. S. Furumoto, Microearthquake survey of the east rift zone of Kilauea, Puna, Hawaii; (abstract) *Trans. Am. Geophys. Union*, v. 56, p. 397, 1975.
- Talwani, M., J. L. Worzel and M. Landisman, Rapid gravity computations for two-dimensional bodies with applications to the Mendocino Submarine Fracture Zone; *Jour. Geophys. Res.*, v. 64, p. 49-59, 1959.
- Tilling, R. I., R. Y. Yoyanagi, P. W. Lipman, J. P. Lockwood, J. G. Moore and D. A. Swanson, Earthquake and related catastrophic events, Islands of Hawaii, November 29, 1975; A preliminary report, Geological Survey Circular, 740, 1976.
- Vacquier, V., N. C. Steenland, R. G. Henderson and I. Zietz, Interpretation of aeromagnetic maps; *Geol. Soc. Am. Mem.*, 47, 1951.
- Wright, T. L., W. T. Kinoshita and D. I. Peck, March 1965 eruption of Kilauea volcano and the formation of Makaopuhi lava lake; *Jour. Geophys. Res.* 73, p. 3181-3205, 1968.
- Zablocki, C. J. and R. I. Tilling, Field measurements of apparent Curie temperatures in a cooling basaltic lava lake, Kilauea Iki, Hawaii; *Geophys. Res. Lett.*, v. 3, p. 487-490, 1976.